Novel Designs for Ion Mobility Spectrometry/Time-of-Flight Mass Spectrometry

Samuel I. Merenbloom
Clemmer Group

Submitted 22nd April, 2005 to Indiana University Department of Chemistry
in partial fulfillment of the requirements for C500.

Contents

List of Figures

Figures, cont'd

Preface

This paper contains a summation of all that has been done this past year. It includes a small experiment performed over the summer, as well as two newly proposed drift tube designs. As is the case with other design-heavy papers, this one will focus on the factors considered in both design processes, and most of the data represented will be computer simulations as well as design drawings. My purpose with this paper is to show what I have learned in this past year, and to show what I propose to do with the rest of my time at Indiana University.

I. Introduction

Ion mobility spectrometry (IMS), although not a relatively recent development, is a technique finding renewed interest from the proteomics community. Since it's advent in 1970 under the guise Plasma Chromatography,[1] IMS has been used to analyze volatile hydrocarbons, separate isomeric compounds, and most recently, to help characterize complex protein mixtures. The concept behind IMS is a relatively simple one. A drift tube (normally of a stacked electrode design) is filled to a certain pressure (up to an atmosphere) with an inert drift gas. A voltage gradient is then applied to the drift tube, causing the ions to travel the length of the drift tube. As they traverse the drift tube, the ions separate based on two factors: (1) ions with a greater charge feel the electric gradient more than ones with less charge, and (2) larger, bulkier ions experience more collisions with the inert drift gas, slowing them down relative to smaller, more compact ones.

IMS has several advantages that have made it an attractive alternative or supplement to conventional separation techniques as a proteomics tool. Perhaps the most striking advantage is the speed of separation. While a typical HPLC experiment can last up to 30 minutes, an IMS experiment only lasts on the order of milliseconds, plus tens of microseconds more if coupled to a time-of-flight mass spectrometer. This leads to many more theoretical plates per second for IMS, 2.6 million per second as opposed to tens of plates per second for HPLC and hundreds of plates per second for GC and capillary electrophoresis.[2] In addition, IMS adds another dimension of separation to an LC-MS experiment, separation of ions based on their size and charge. This eliminates many isobaric overlaps from occurring, and allows fragment ions to be mobility labeled to their precursor (if fragmentation is induced at the end of the drift tube), an advantage over many scanning techniques. This allows for many more hits in a database search.

The initial goal of my C500 research was to optimize fragmentation at the front of a drift tube in the efforts to study the structural differences of b and y ions formed by the fragmentation of peptides and proteins. This phenomenon would yield a "fingerprint" region in a mobility spectrum for every protein and peptide. Therefore, this approach could be used for rapid sequencing or database identification of proteins separated by liquid chromatographic means in a proteomics experiment. My research then extended towards the design of new IMS instrumentation, for improved fragmentation efficiency and resolution.

Research at Indiana University utilizing ion mobility has contributed myriads of data regarding the structures of peptides and proteins in the gas phase.[3, 4, 5, 6] Work in this area shows the structures are organized into several comformer types, including: α-helices, globules, and those with collision cross-section in between.[4] Several factors have been identified that influence the formation of helices: the predilection of the constituent amino acids to form helices; the contributions of charged residues to the overall dipole of the helix; capping interactions at the N- and C-termini; and the interactions of the side chains of adjacent amino acids in the helical turn.[6] Extensive research in the Clemmer group shows that the i $\rightarrow$ i+4 interaction strongly influences the formation of helices, including acidic-basic, polar-polar, aromatic-basic, and nonpolar-nonpolar interactions all being amenable to helix formation.[6] At least five amino acids with favorable interactions are necessary for a turn, with the most noticeable conformation changes occurring around fifteen residues. Therefore, it would be feasible to separate large fragment ions formed at the front of a drift tube based on their differing conformations.

The formation of signature ions (a/x, b/y, c/z) during the subjection of proteins and peptides to mass spectrometry is a well-observed phenomenon.[7, 8, 9] The most common fragments observed are b and y ions, which involve cleavage of the amide bond.[10, 11] Prior research by the Wysocki group has shown that amino acid composition greatly influences the presence of b and y ions in the fragmentation spectrum of a protein or peptide.[11, 12] More specifically, a basic residue (Arg, Lys, His) closer to the N-terminus leads to a predominance of b ions, while tryptic peptides or proteins (those that have a C-terminus Arg or Lys) typically produce more y ions. This is believed to be due to the basic side chain sequestering a proton during the fragmentation process.

Initial examination of biomolecular mixtures using IMS-TOF in the Clemmer group involved the utilization of an ion trap at the front of the drift tube.[13] Using the ion trap to accumulate electrosprayed ions for injection into the drift tube, they were able to identify many of the peptides from the tryptic digest of cytochrome c from data acquired in under a minute. In addition to accumulation, an ion trap can be utilized for the fragmentation of proteins before the drift tube, allowing the fragments to be mobility separated.[14] This allows collision cross-sections to be obtained for structural elucidation.

For example, Badman *et al* utilized fragmentation in an ion trap with SWIFT excitation at the front end of a drift tube to study the mobility of insulin chain b fragments.[15] Fragmentation of the protein yielded much information; however, the signal obtained was low, due to the lack of focusing of the ion cloud prior to entry of the drift tube. In addition, the full sequence of fragments was not covered, due to the ejection of low m/z ions from the trap because of their lack of stability.[16, 17]

In addition to the loss of low mass fragment ions, CID in an ion trap is incapable of fragmenting ions of high m/z.[18, 19, 20, 21, 22] The collision energy of an ion is directly proportional to the square of its charge.[20] Therefore, for ions of a given mass, fragmentation efficiency increases with increasing charge, with singly and doubly charged ions proving most difficult to fragment. One of the experimental sections in this paper will focus on utilizing IMS-TOF to probe the structural differences of b and y ions formed in an electrodynamic ion funnel at the front of a drift tube. The ion funnel refocuses ions to a narrow beam, allowing for an enhancement in signal. In addition, research in the Smith group has shown that a high RF voltage on the funnel leads to CID of lower m/z ions near the exit orifice.[23, 24]

Several researchers have displayed that fragmentation can be produced at the interface of a nozzle and skimmer cone of an atmospheric electrospray ionization source by increasing the voltage difference between the two electrodes.[25, 26] By giving the ions a larger amount of kinetic energy while sending them through a pressure drop, it is possible for the ions to have numerous low-energy collisions, leading to fragmentation.[25] As opposed to ion trap CID, this method allows for the transmission and detection of low m/z fragments, and therefore greater sequence coverage.

The Clemmer group took advantage of this phenomenon to induce fragmentation at the exit of the drift tube, in a differentially pumped region prior to the time-of-flight region.[10, 27] The current split-field drift tube geometry used in the Clemmer group utilizes this concept.[10] Ions are mobility separated in the low-field region, then transmitted through a second region, which is controlled by the difference in the potentials of the conical lens and the beryllium/copper (BeCu) plate. The resulting field is balloon-

shaped, and can be set to either transmit or fragment ions. However, collisions in the high-field region are still not energetic enough to fragment larger, singly and doubly charged precursor ions.[10,18, 19, 20, 21, 22] In addition, fragments are formed at the rear of the drift tube, and are therefore not mobility separated from one another.

The second experiment outlined in this paper describes the design of a modified split-field region, which could be used at either end of the drift tube. This would allow for either mobility selective accumulation of ions, or improved fragmentation efficiency of proteins and peptides at both ends, introducing the possibility for quick sequencing and MS^n experimentation within a drift tube.

The last experimental section focuses on the development of a curved drift tube in the efforts to build a high-resolution, low-pressure drift tube (high resolution IMS instruments are those in which resolution exceeds 100). Resolution in IMS is examined in a manner very similar to other chromatographic methods. The most common resolution calculation used is the single peak resolution, or resolving power[2]:

$$R_p = \frac{t_d}{w_h} \tag{1}$$

where t_d is the drift time of the ion, and w_d is the width of the ion pulse measured at half the maximum. The width at half maximum can be conveniently used without any coefficient because the peak width in IMS occurs at 6.25% of the maximum, as opposed to 13.4% in other chromatographic methods. This easily coincides with twice the width at half maximum.[28] The width at half maximum is simply the width of the initial pulse of ions, plus the change in width of the ion packet due to diffusion over it's time in the drift tube, $t_{d:}$[2, 28, 29]

$$w_h^2 = t_g^2 + \left(\frac{16k_bT\ln 2}{Vez}\right)t_d^2 \quad (2)$$

where w_h is the width of the ion packet after it's drift time t_d, t_g is the width of the gating pulse, k_b is the Boltzmann constant, T is the temperature, V is the voltage applied to the drift tube, e is the charge of an electron, and z is the numerical charge of the ion. Siems *et al*[30] applied a modified version of equation (2) with three adjustable parameters to a series of singly charged ions to find the best fit:

$$w_h = \gamma + \beta t_g^2 + \left(\frac{\alpha T}{V}\right)t_d^2 \quad (3)$$

where w_h, t_g, T, V, and t_d are defined as in equation (2). γ represents changes in peak widths due to collector and amplifier rise times, while β represents Coloumbic repulsion during the gating of ions into the drift tube, and α represents inhomogeneities in the electric field of the drift tube, which is a function of the diameter of the drift tube.

Examination of equations (2) and (3) show that there are ultimately two variables that can be changed in order to increase resolution: the drift voltage and temperature. Although equation (1) suggests that observing ions with longer drift times (or just lengthening the drift tube) will lead to an increased resolution, equations (2) and (3) show that the peak width increases with the square of the drift time, leading to a decrease in resolution. This is due to diffusion of the ion packet, as explained below.

Voltage is a parameter that requires some thought. Although equations (2) and (3) suggest that a higher voltage leads to a greater resolution, there are several reasons voltage cannot be raised without either lengthening the drift tube or increasing the drift gas pressure. First, increasing the voltage of the drift tube also increases the electric field strength of the drift tube:

$$E = V / L \tag{4}$$

For all drift gases, there is a maximum electric field that can be reached before electrical breakdown.[31, 32] Therefore, if one wants to increase the voltage, they also need to increase the length of the drift tube if they wish to maintain a constant E. In addition, the most common practice is to operate in the low-field regime, in which the ion velocity remains proportional to the electric field.[29, 32] This requires the ratio of the electric field, E, to the number density of the drift gas, N, to remain around 1-2 Td (1 Td = 1 x 10^{-17} V/cm^2), depending on the m/z of the ion. If the drift pressure were fixed (say, at one atmosphere, where N = 2.46 x 10^{19} cm^{-3}), this means E would have to be between 246 and 493 V/cm.[32] With pressure fixed, an increase in voltage would mean an increase in length as well, to maintain E/N. Lastly, a larger voltage without an increased drift tube length leads to a greater contribution of t_g to the peak width, since the t_d contribution is inversely proportional to voltage (equations (2) and (3)). Consequently, for any given t_g, there's an optimal voltage to maximize resolution:[30, 32, 33]

$$V_{opt} = \left(\frac{\alpha T L^2}{2\left(\gamma + \beta t_g^{\,2}\right)^{1/2} K^2} \right)^{1/3} \tag{5}$$

However, for singly charged ions, it is often necessary to work at a voltage above V_{opt} in order to have adequate signal.[32] Alternatively, the pressure of the drift tube can be increased along with the voltage, while keeping the length constant. Several atmospheric-pressure drift tubes have been constructed, yielding resolutions an order of magnitude greater than their low-pressure counterparts have.[32, 34, 35, 36] For our purposes, though, the pressure of the drift tube must be relatively low (~3-4 Torr) in order to

maintain high fragmentation efficiency at the exit of the drift tube.[10] Therefore, the other option is to increase the drift tube length.

Increasing the length of the drift tube in order to increase resolution has one major setback: diffusion. The effects of diffusion on an IMS experiment can be examined in a matter very similar to most chromatographic methods.[29] The initial pulse of ions into the drift tube can be treated as an infinitely narrow pulse (a Dirac function). As the ion packet travels the length of the drift tube, diffusion causes it to broaden to a finite width (a Gaussian distribution). If only motion in the x-direction is considered, then the number of ions through a cross-sectional area of the drift tube at a given time is equal to the number of ions at the initial pulse minus the number of ions that have spread from the pulse center due to diffusion. Therefore, the following relation can describe the flux of ions, J:

$$\mathrm{J} = nKE - D\frac{\partial \mathrm{n}}{\partial \mathrm{x}} \tag{6}$$

in which n is the number density of ions, and D is the diffusion coefficient. This equation applies to all situations, but for ease of calculation, equilibrium will be chosen. At equilibrium, the diffusion of ions exactly balances the flow caused by the electric field. Therefore, J = 0, and n can be described by the following Boltzmann exponential:

$$n = n_0 \mathrm{e}^{\mathrm{qEx/kT}} \tag{7}$$

where q = ze, the charge of the ion. Differentiating equation (7) gives ($\partial n/\partial$x):

$$\frac{\partial n}{\partial x} = n\frac{qE}{k_b T} \tag{8}$$

Substituting equation (8) into equation (6), and setting J = 0 gives the Nernst-Townsend-Einstein relation for the mobility of an ion in a vanishing electric field:

$$K = \frac{qD}{k_b T} \tag{9}$$

For a fixed mobility and temperature, the diffusion coefficient is approximated for low-field conditions by rearranging the Nernst-Townsend-Einstein relation:

$$D = \frac{Kk_b T}{e} \tag{10}$$

For two and three dimensions, the root-mean-square displacement can be approximated by:[37]

$$\sqrt{r^2} = \sqrt{4Dt} \quad \text{(2D)}$$
$$\sqrt{r^2} = \sqrt{6Dt} \quad \text{(3D)} \tag{11}$$

where r is the mean displacement of the ion packet, D is the diffusion coefficient, and t is the drift time. If length is the only variable changed, then elongating the drift tube leads to an increased drift time, which leads to greater diffusion in all three dimensions. Therefore, there is a terminal length and time at which the ion packet diffuses to the radius of the drift tube electrode, leading to signal loss and inhomogeneity in the field due to charging.

Until recently, the only way around the diffusion limit was to increase the diameter of the drift tube electrode, although this leads to problems with electric field homogeneity and detection.[32] Currently, efforts are being taken to utilize electrodynamic ion funnels to refocus an ion beam to a diameter much smaller than that of the drift tube electrode.[23, 38, 39] Spacing funnels at the diffusion-limited distance can refocus ions, allowing for drift tubes much longer than the current designs.

II. Experimental

Conformational differences of b and y ions

Experimentation was carried out on an ion mobility spectrometry/time-of-flight (IMS-TOF) mass spectrometer with an ion funnel at the front end of the drift tube as shown in Figure 1. The electrodynamic ion funnel was used for fragmentation and focusing of ions into the drift tube.[23, 24, 38] As explained in the Introduction, a high RF voltage on the funnel leads to CID of lower m/z ions near the exit orifice.[23, 24] After fragmentation in the ion funnel, ions were introduced to the drift tube for mobility separation, followed by orthogonal ejection into a time-of-flight mass spectrometer with reflectron geometry for m/z analysis.

Fragmentation studies used ubiquitin (Sigma Aldrich, MQIFVKTLTGKTITLEVEPSDTIENVKAKIQDKEGIPPDQQRLIFAGKQLEDGRTLS DYNIQKESTLHLVLRLRGG; 8559.6145 Da) at a concentration of 0.01 mg/mL in a solution of 49:49:2 HPLC grade water: HPLC grade acetonitrile: acetic acid. Data were collected for an hour each with the RF peak-to-peak voltages at values of 15, 50, and 83.3 V, with a DC field gradient of ~14 V/cm. All other conditions were kept constant.

Modeling of novel drift tube designs

The first part of this project includes a modified split-field drift tube design that can be used for mobility-selected trapping of ions for subjection to further mobility studies or increased fragmentation efficiency. The split-field drift tube design shown in Figure 2 was taken as a starting point due to its simplicity as well as its ability to refocus ions in the balloon field.[10, 27] The modified design was created by removing the skimmer cone, and adding a set of oppositely facing conical lenses. Modifications to this

geometry were studied using SIMION 7.0.[40] A resolution of 1/32" per grid unit was used, and the optimal distance between the conical lenses and the beryllium/copper plate were determined previously.[10]

The second experiment represents the first step in the efforts towards building a space-saving, high-resolution, long-length drift tube. All modeling was performed using SIMION 7.0, at a resolution of 1/32" or 1/16" per grid unit, the latter being used when a full 180° was modeled. An additional program, which took collisions with the buffer gas into account, was used in conjunction with all SIMION calculations. This program subtracts a constant value from the velocity of each ion for each time τ, which is defined by the user. SIMION also accounted for coloumbic repulsion within the ion packet. In all cases, the ions were flown from right to left (counterclockwise around the turn).

Several factors were considered in the design of the curved drift tube. The key factor in the determination of the angle chosen for the spacer was its thickness around the inner part of the turn (the inner distance between adjacent electrodes had to be large enough to accommodate exterior connections and ensure adequate strength of the delrin spacer). To maintain the same electrode size as a straight drift tube, the electrode inner and outer diameter of 2.75" and 5.00" were used. In addition, the turn had to be compact, yet capable of sustaining a drift field sufficient to turn the ion beam. Lastly, to keep construction at a minimum, the number of electrodes was an integral dividend of 180.

To ensure that field homogeneity did not vary greatly with a change in the angle between adjacent electrodes, several angles were modeled. An eighty-eight degree turn taken at four degree increments was modeled at a resolution of 1/32" per grid unit, and a one hundred and eighty degree turn taken at both eight and ten degree increments were

modeled at a resolution of 1/16" per grid unit. In each instance, a drift field of approximately 10 V/cm was maintained around the inner diameter of the turn. Ion trajectories were modeled using both the linear dampening program in conjunction with SIMION's own Coloumbic repulsion algorithm. Fifty singly charged 1000 Da ions originated from a point source, located at the midpoint of the drift electrode in each instance. The effects of changing the mass to charge ratio were also examined, using a ten-degree spacer. Fifty ions each, of 250, 500, 1000, and 2000 Da, all singly charged, were flown from a point source.

A final SIMION experiment examined the effect of the ion packet diameter on its temporal resolution. Packet sizes of 0.005", 0.010", 0.100", 0.200", 0.300", 0.400", and 0.500" were modeled. In each instance, the number of ions flown was equal to the number of thousandths of inches wide the packet was (i.e., a packet of 0.200" contained 200 ions). To maintain constant space charge effects, the distance between ions was held constant at one thousandth of an inch. Singly charged ions of both 1000 and 500 Da were flown in individual trials, to observe if any mass discrimination existed. The temporal resolution was measured as the difference in time between the slowest and fastest ions.

Calculations for the diffusion of the ion beam as it traversed the drift tube were performed using a C++ program written in-house, which calculated the diffusion coefficient using equation (19). The singly charged bradykinin (RPPGFSPFR, 1060 Da) ion was used as a model. The mobility constant in equation (19) can be determined either experimentally or from theory. If the ion is assumed spherical, then the mobility can be approximated by Stokes' Law[41]:

$$K = \frac{1}{6\pi\eta R} \tag{12}$$

where R is the radius of the ion, and η, the gas viscosity, can be calculated from kinetic theory:

$$\eta = \frac{1}{2} nm < v > l \tag{13}$$

in which n is the number density of the gas molecules, m is the molecular mass of the gas, $<v>$ is the mean molecular speed, and l is the mean free path. Solving equations (13), (12), and (11) will provide a rigorous determination of the theoretical size of an ion packet after its time through a drift tube.

The size of an ion packet of a given drift time can also be roughly calculated by dividing the length of the drift tube by the resolution of the ion. This can be explained by re-examining equation (14):

$$R_p = \frac{t_d}{t_{1/2}}$$

where $t_{1/2}$ is now used to represent the width of the ion pulse at half maximum. Through diffusion, this is also equal to the distance traveled by the ion packet (or the length of the drift tube) divided by the change in its width:

$$R_p = \frac{t_d}{t_{1/2}} = \frac{L}{\Delta L} \tag{14}$$

Then, to get the full width of the ion packet, one simply needs to multiply by two, since this represents half the width of the Gaussian distribution.

Since the angle and number of electrodes did not have a significant impact on the ion trajectories in SIMION, the C++ program was used only for the eight-degree spacings. As described above, the diffusion of the ion packet was analyzed in three different ways. The radius of the singly charged bradykinin ion was calculated from the

known collision cross section for the ion (242 $Å^2$), assuming it was spherical. Then, the viscosity was calculated using equation (22), assuming helium to be the drift gas at a pressure of 2 torr. Lastly, the mobility was calculated via equation (21). Alternately, the diffusion coefficient was calculated directly using an experimentally determined mobility for the ion (0.0606 m^2/Vs). A larger diffusion coefficient was obtained via the first method (1.57×10^{-3} m^2/s), and this value was used for the simulation.

III. Results and Discussion

Fragmentation of ions in an ion funnel

For these studies a small protein, ubiquitin, was used to probe the ability of an ion guide to induce fragmentation. At an RF of 15 V (Figure 3), a precursor ion spectrum is obtained, with little fragmentation observed, as shown in the mass spectra to the right. At both 50 V (Figure 4), several b and y "series" are observed, barely above the noise. An increase to 83 V more fragments are observed in Figure 5. However, the higher RF also yields more internal (i.e. higher energy) fragments, possibly from secondary fragmentation. As the mobility spectra in Figures 4 and 5 show, it is difficult to observe where the b and y ions are in mobility, due to the relative intensities of the most prevalent ions. Further enhancements, in both fragmentation efficiency and data presentation, will be performed in the future.

SIMION mapping of newly designed split-field drift tube

The modified split-field drift tube design can be seen in Figure 6. The skimmer cone was replaced with a set of oppositely facing conical lenses. The advantage of this design is that it can produce two focusing balloon fields in either direction. Figure 7

shows the fields produced with the geometry at the front of the drift tube, while Figure 8 shows the resulting fields for the geometry at the rear of the drift tube. In both cases, the quality of both ballooning fields is comparable to that in Figure 2. In addition, the strength of either balloon field can be altered independent of the other (not shown). As opposed to one high field region, two can now be produced, with comparable focusing in either direction. In addition, although the pressure of the differentially pumped region is not well defined, the pressure decreases from the first high-field region to the second (see Figures 6 and 7), allowing for more low-energy collisions. This could possibly lead to fragmentation of singly and doubly charged ions.

SIMION and advanced computational studies and design of curved drift tube

A diameter of 13.4 inches (as measured from the center of the first electrode in the turn to the center of the last electrode) and an angle of 10 degrees were ultimately chosen. This resulted in 18 spacers, 0.6691" thick along the inner part of the curve. At a 13.4" diameter, the length of the drift tube (taken as the circumference of the turn at the midpoint of the electrode) was calculated to be 53.5 centimeters.

The study of the effects of the drift spacer angle on field homogeneity and ion trajectory an be seen in Figures 9 through 11. The slight ballooning fields shown at the ends of the drift tubes are artifacts of the geometry file, and do not exist in the real drift tube. As can be seen, the homogeneity of the field and the ion trajectories were not altered with the change in angle or number of electrodes. In addition, since the electrodes were all of the same radius, the drift fields along the inside and outside of the curve were the same in each case. Therefore, ten-degree spacers were chosen, since they required the least number of spacers for construction.

Figure 12 shows the trajectories of ions of several m/z values through the curved drift tube. The ions changed trajectories slightly going through the turn, with the lightest ions having the longest trajectory. This arises from the differing field strengths at the inner part of the turn versus the outer region. Due to the greater spacing between electrodes along the outer part of the curve, the electric field is weaker than along the inside of the curve, where the electrodes are closer together. The higher field along the inside of the curve accelerates ions of lower m/z farther than those with higher m/z. However, as can be seen in the figure, this effect is minimal for ions introduced at the center of the drift tube.

Temporal resolution as a function of ion packet width can be seen in Figure 13. It can be seen that as the ion packet diameter increases, the resolution decreases in a linear fashion, since (Δt) in equation (14) is increases. This is again due to the differing fields along the inside and outside of the curve. Ions along the inside of the curve experience a greater drift field than ions along the outside of the curve, and therefore are accelerated more than their counterparts. Ions of low m/z are more subject to this phenomenon, due to their greater velocities, resulting in the steeper slope for m/z 1000 as opposed to m/z 500. Obviously, the wider the ion packet, the greater the difference becomes. Therefore, it will be desirable to focus the ion beam to the smallest radius possible prior to entry of the curve, using an ion funnel. The current ion funnel design employs an exit aperture of 0.2", which may need to be redesigned. However, the SIMION simulation did not provide an exact measure of pressure, only a very rudimentary linear dampening calculation.

The result of the diffusion simulation is shown in Figure 14. As can be seen, although the ion cloud diffuses during its flight, its size never comes close to the inner radius of the drift electrode. Since the SIMION file was plotted at a resolution of 1/16" per grid unit, the estimated size of the ion packet at the final electrode is 1.6875" (as opposed to 2.75", the inner diameter of the drift electrode). This figure is slightly larger than the value obtained using equation (22) for a singly charged bradykinin ion of typical resolution (~30) traversing a 54 cm drift tube (approximately 1.42"). This discrepancy is again believed to be due to the differences in field strengths at the inner part of the turn versus the outer part of the turn.

Design drawings for the two drift tube spacers and electrode as well as photographs of the finished products can be seen in Figures 15-20. A two spacer system, in which the top spacer screws onto the bottom one, was chosen, for ease of construction as well as guaranteed o-ring compression. It can be seen in Figures 15 and 16 that both spacers have the same bolt-hole pattern, only the recesses to accommodate the bolt heads are offset by ninety degrees from one spacer to the next. Figure 18 shows how the spacers connect to assemble the drift tube. The dimensions of these pieces are comparable to those of their straight drift tube counterparts, allowing for easy connection between tubes.

IV. Future Directions

Regarding fragmentation of large peptides and proteins in an ion funnel, several options are available. Recently, we have discovered that frequency also influences the fragmentation of ions in a funnel. Optimization of the frequency, RF amplitude, and DC

field will be studied to control fragmentation in an ion funnel. Should this prove inefficient, alternative methods, including the modified split-field drift tube, will be tested. Ultimately, relationships between mobility and structure of large fragment ions will be investigated.

With respect to the split-field drift tube, this design could be utilized in two different ways. One use for this geometry could be mobility-selected trapping and accumulation of an ion packet for selected transmission into further stages of analysis, in which the fields at the front and back of the drift tube switch as the ion of interest traverses the length of the accumulation region. This can have numerous uses, in physical chemistry, proteomics, and chemical arms detection.

Placement of this geometry between two drift tubes allows for drift-drift experimentation as outlined in Figure 21. The front of the first drift tube can be operated to either transmit precursor ions (A, B, and C) or produce and transmit fragment ions (D, E, and F). Keeping both the middle and rear at low-field conditions (A) allows low-field mobility and m/z analysis of precursor ions. Operating the middle region at high-field conditions while keeping the rear at low field (B) permits low-field mobility analysis of both precursor and fragment ions, as well as m/z analysis of fragment ions (MS^2). Running both regions at high-field conditions (C) produces low-field mobility analysis of both the precursor and fragment ions along with m/z analysis of the fragments of the fragments (MS^3). A high field at the front followed by low fields (D) permits low-field mobility and m/z analysis of fragment (MS^2) ions. High fields at the front and middle regions (E) allow for mobility studies of both MS^2 and MS^3 fragment ions, with m/z analysis of MS^3 fragments. Operation of the first two regions at high field with the final

region low allows production, m/z analysis, and drift analysis of MS^3 ions. Three more possibilities, including MS^4, are not shown. Each of these experiments could be performed on a time-scale amenable to coupling with chromatographic separations, making myriads of data accessible.

Studies utilizing the 180° curved drift tube are soon to be underway. Once mobility around the curve is characterized and optimized, it will be possible to construct a drift tube as shown in Figure 22. Placement of ion funnels before and after the curved regions allows for radial compression of the ion packet, reducing signal loss and the problem described in the Experimental section. Elongation of the drift tube will lead to higher resolutions and better separations.

The advancement of drift tube lengths and ion refocusing elements also makes possible a joint effort that has been considered for a while by the Clemmer and Marshall groups: the coupling of Ion Mobility to Fourier Transform Ion Cyclotron Resonance Mass Spectrometry (FT-ICR MS). FT-ICR MS provides the best resolution and mass accuracy of any mass spectrometric method. In addition, the capability to store ions inside the ICR cell while imparting them with energy allows for the fragmentation of macromolecular systems typically not fragmented with other methods[42]. FT-ICR MS has been coupled to numerous MS^n techniques, including electron capture dissociation (ECD) and infrared multiphoton dissociation (IRMPD)[42, 43, 44]. Perhaps the most attractive feature of this technique is the complementary data provided by the different fragmentation schemes; ECD allows for elucidation of the precursor ions structure[43], while IRMPD provides more sequence coverage[44].

The concept would be to place a drift tube in front of an ICR cell, allowing for accumulation and study of a particular conformation, as shown in Figure 23. This can be used to select a particular conformation for ECD analysis, allowing for structure-specific fragmentation pathway studies. On the other hand, a particular unknown peptide or protein can be chosen for IRMPD analysis for sequence coverage. Additionally, various excitation methods could be employed within the ICR cell to eject fragment ions back into the drift tube, for further cross-sectional analysis (requiring a setup slightly different from Figure 23). Greater control of ions entering the ICR cell makes a myriad of experiments feasible.

V. Acknowledgements

There is not enough space to thank everybody that has helped me this semester, so hopefully no one will be offended. Of course, many thanks to Dr. Clemmer, for his support. I would like to thank the Clemmer group for accepting me into their ranks for this past year. In particular, I would like to thank Dr. Steve Valentine for his assistance, Stormy Koeniger for her patience, and Amy Hilderbrand for her humor and advice. The curved drift tube would not have been possible without the Edward J. Blair Instrumental Shop, particularly Rick Moore. The Electronics Instrumentation Services crew also deserves notice. Lastly, I would like to thank my incredibly cool fiancé, for putting up with me.

VI. References

1. Cohen, M. J.; Karasek, F. W. *Journal of Chromatog. Sci.*, **1970,** *8*, 330.

2. Asbury, G. R.; Hill, H. H. Jr. *J. Microcolumn Separations.* **2000,** *12*, 172.

3. Breaux, G.A.; Jarrold, M.F. *J. Am. Chem. Soc.* **2003,** *125*, 10740.

4. Counterman, A.E.; Clemmer, D.E. *J. Phys. Chem. B* **2004,** *108*, 4885.

5. Myung, S.; Badman, E.R.; Lee, Y.J.; Clemmer, D.E. *J. Phys. Chem. A* **2002,** *106*, 9976.

6. Srebalus Barnes, C.A.; Clemmer, D.E. *J. Phys. Chem. A* **2003,** *107*, 10566.

7. Biemann, K. *Methods Enzymol.* **1990,** *193,* 351.

8. Ballard, K.D.; Gaskell, S.J. *Int. J. Mass Spectrom. Ion Processes* **1991,** *111*, 173.

9. McCormack, A.L.; Somogyi, Á.; Dongré, A.R.; Wysocki, V.H. *Anal. Chem.* **1993,** *65*, 2859.

10. Valentine, S.J. ; Koeniger, S.L.; Clemmer, D.E. *Anal. Chem.* **2003,** *75*, 6502.

11. Tabb, D.L.; Smith, L.L.; Breci, L.A.; Wysocki, V.H.; Lin, D.; Yates III, J.R. *Anal. Chem.* **2003,** *75*, 1155.

12. Tabb, D.L.; Huang, Y.; Wysocki, V.H.; Yates III, J.R. *Anal. Chem.* **2004,** *76*, 1243.

13. Henderson, S. C.; Valentine, S. J.; Counterman, A. E.; Clemmer, D. E. *Anal. Chem.* **1999,** *71*, 291.

14. Fukui, K.; Naito, Y.; Akiyama, Y.; Takahashi, K. *Int. Journal Mass Spectrom.* **2004,** *235*, 25.

15. Badman, E.; Myung, S.; Clemmer, D. E. *Anal. Chem.* **2002,** *74*, 4889.

16. Payne, A. H.; Glish, G. L. *Anal. Chem.* **2001,** *73*, 3542.

17. Hashimoto, Y.; Hasegawa, H.; Yoshinari, K.; Waki, I. *Anal. Chem.* **2003,** *75*, 420.

18. Loo, J. A.; Udseth, H. R.; Smith, R. D. *Rap. Commun. Mass Spectrom.* **1988,** *2*, 207.

19. Loo, J. A.; Edmonds, C. G.; Smith, R. D. *Science.* **1990,** *248*, 201.

20. Loo, J. A.; Edmonds, C. G.; Smith, R.D. *Anal. Chem.* **1993,** *65*, 425.

21. Gabryelski, W.; Li, L. *Rev. Sci. Instum.* **1999,** *70*, 4192.

22. Gabryelski, W.; Li, L. *Rap. Commun. Mass Spectrom.* **2002,** *16*, 1805.

23. Shaffer, S. A.; Tang, K.; Anderson, G. A.; Prior, D. C.; Udseth, H. R.; Smith, R. D. *Rapid Commun. In Mass Spectrom.,* **1997,** *11*, 1813.

24. Schaffer, S. A.; Prior, D.C.; Anderson, G.A.; Udseth, H.R.; Smith, R.D. *Anal. Chem.* **1998,** *70*, 4111.

25. Smith, R. D.; Loo, J. A.; Baringa, C. J.; Edmonds, C. G.; Udseth, H. R. *J. Am. Soc. Mass Spectrom.* **1990,** *1*, 53.

26. Schneider, B. B.; Chen, D. Y. *Anal. Chem.* **2000**, *72*, 791.

27. Lee, Y. J.; Hoaglund-Hyzer, C. S.; Taraszka, J. A.; Zientara, G. A.; Counterman, A. E.; Clemmer, D. E. *Anal. Chem.* **2001,** *73*, 3549.

28. Rokushika, S.; Hatano, H.; Baim, M. A.; Hill, H. H. *Anal. Chem.* **1985,** *57,* 1902.

29. Revercomb, H. E.; Mason, E. A. *Anal. Chem.* **1975,** *47,* 970.

30. Siems, W. F.; Wu, C.; Tarver, E. E.; Hill, H. H.; Larsen, P. R.; McMinn, D. G. *Anal. Chem.* **1994,** *66,* 4195.

31. Raizer, Y. P. *Gas Discharge Physics;* Springer-Verlag Berlin Heidelberg: New York, 1997, pp. 128-166.

32. Wu, C.; Siems, W. F.; Asbury, G. R.; Hill, H. H. *Anal. Chem.* **1998,** *70,* 4929.

33. Spangler, G. E.; Collins, C. I. *Anal. Chem.* **1975,** *47,* 403.

34. Dugourd, P.; Hudgins, R. R.; Clemmer, D. E.; Jarrold, M. F. *Rev. Sci. Instrum.,* **1997,** *68*, 1122.

35. Srebalus, C. A.; Li, J.; Marshall, W. S.; Clemmer, D. E. *Anal. Chem.*, **1999,** *71*, 3918.

36. Beegle, L. W.; Kanik, I.; Matz, L.; Hill, H. H. Jr. *Anal. Chem.*, **2001,** *73*, 3028.

37. Mason, E. A.; McDaniel, E. W. *Transport Properties of Ions in Gases;* John Wiley and Sons: New York, 1988, pp. 11-13.

38. Kim, T.; Tolmachev, A. V.; Harkewicz, R.; Prior, D. C.; Anderson, G.; Udseth, H. R.; Smith, R. D.; Bailey, T. H.; Rakov, S.; Futrell, J. H. *Anal. Chem.,* **2000,** *72,* 2247.

39. Belov, M. E.; Gorshkov, M. V.; Udseth, H. R.; Anderson, G. A.; Tolmachev, A. V.; Prior, D. C.; Harkewicz, R.; Smith, R. D. *J. Am. Soc. Mass Spectrom.* **2000,** *11,* 23.

40. Dahl, D.A. *SIMION (Version 7)*: Idaho National Engineering Laboratory: Idaho Falls, ID.

41. Annis, B. K.; Malinauskas, A. P.; Mason, E. A. *Aerosol Sci.,* **1972,** *3*, 55.

42. Laskin, J.; Futrell, J. H. *Mass Spectrom. Rev.* **2005,** *24*, 135.

43. Oh, H.; Breuker, K.; Sze, S. K.; Ge, Y.; Carpenter, B. K.; McLafferty, F. W. *Proceedings of the National Academy of Sciences of the United States of America.* **2002,** *99,* 15863.

44. Little, D. P.; Speir, J. P.; Senko, M. W.; O'Connor, P. B.; McLafferty, F. W. *Anal. Chem.* **1994,** *66*, 2809.

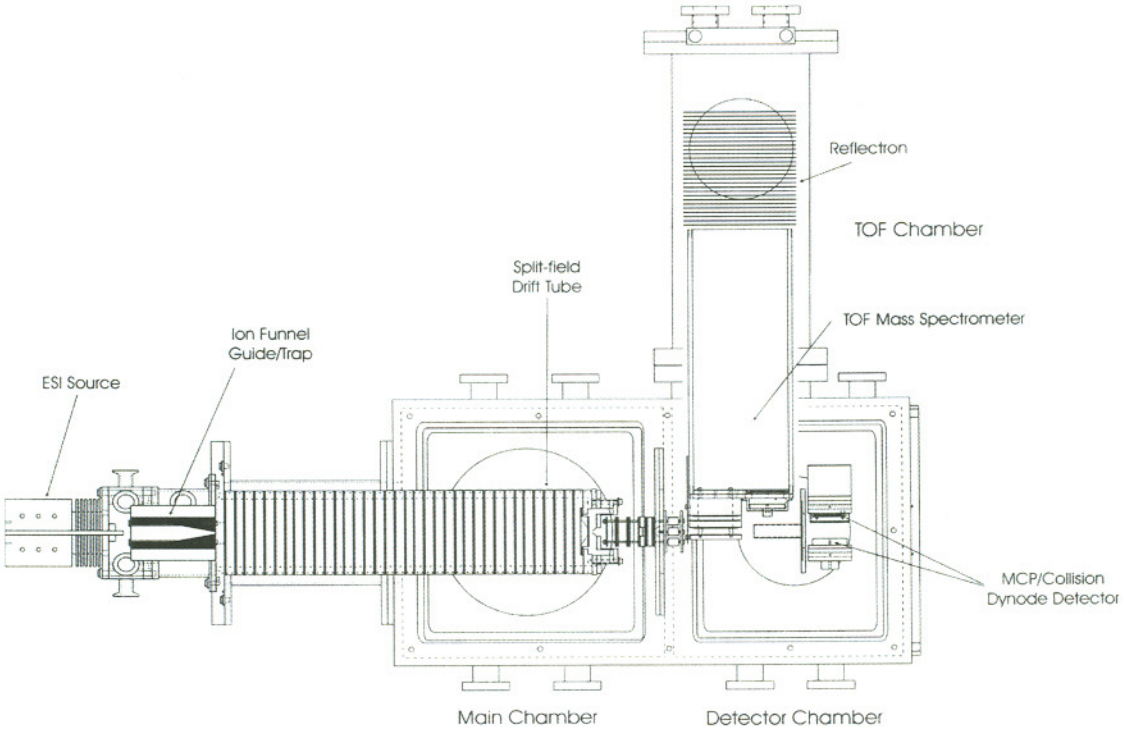

Figure 1: Schematic of IMS-TOF instrumentation with ion funnel after source.

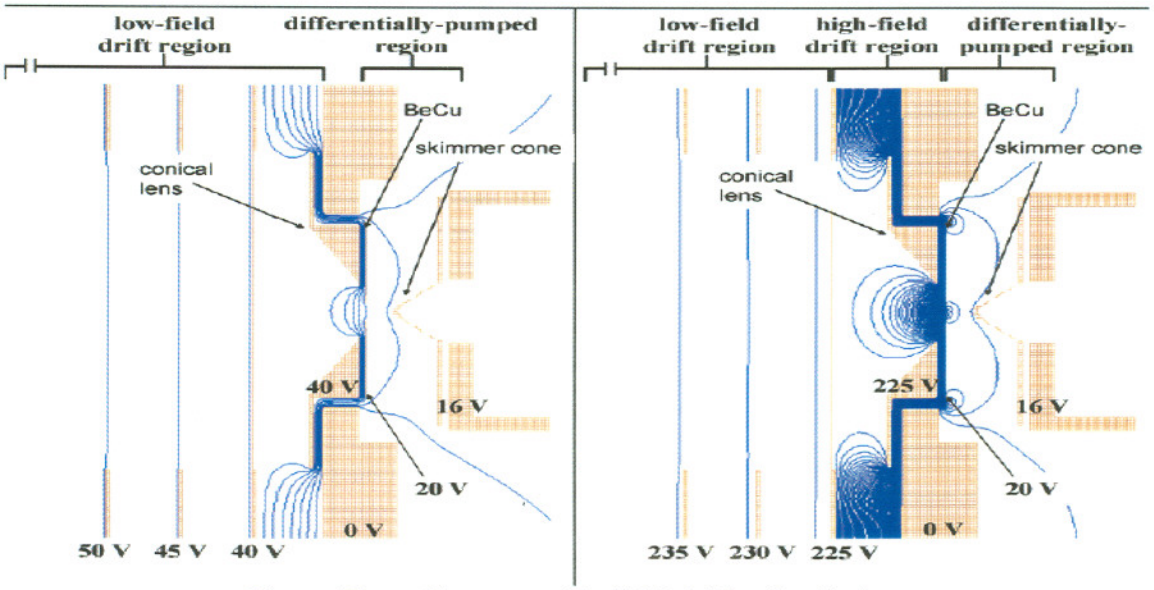

Figure Two: Current split-field drift tube design.

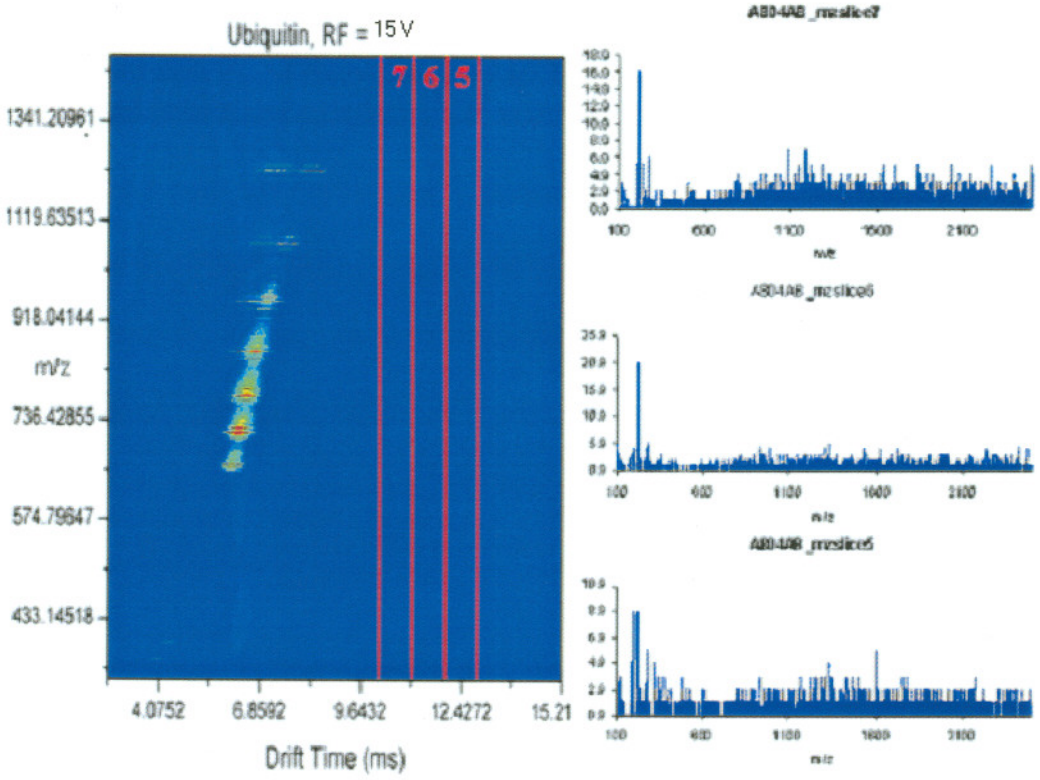

Figure 3: Fragmentation study, funnel RF = 15 V p-p.

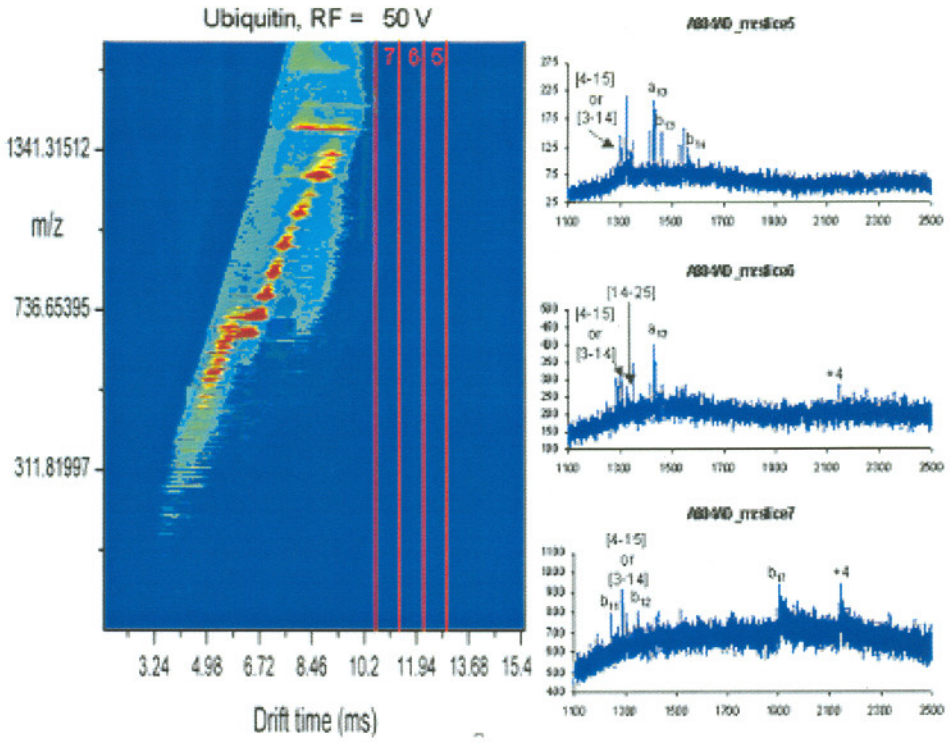

Figure 4: Fragmentation study, funnel RF = 50 V p-p.

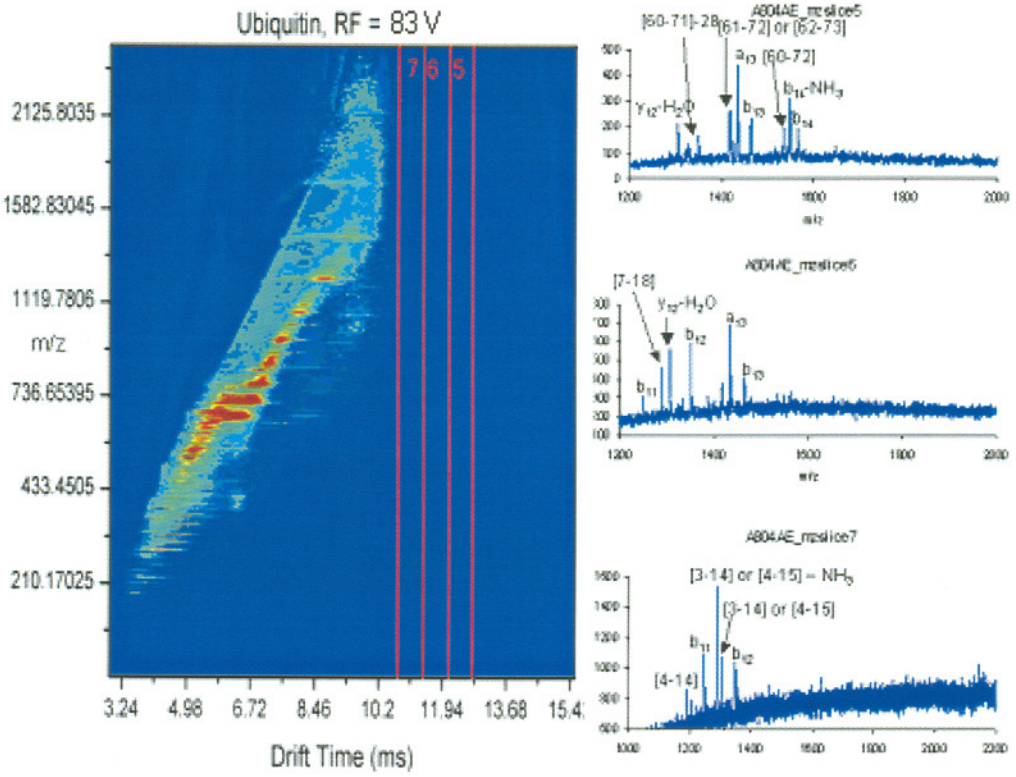

Figure 5: Fragmentation study, funnel RF = 83 V p-p.

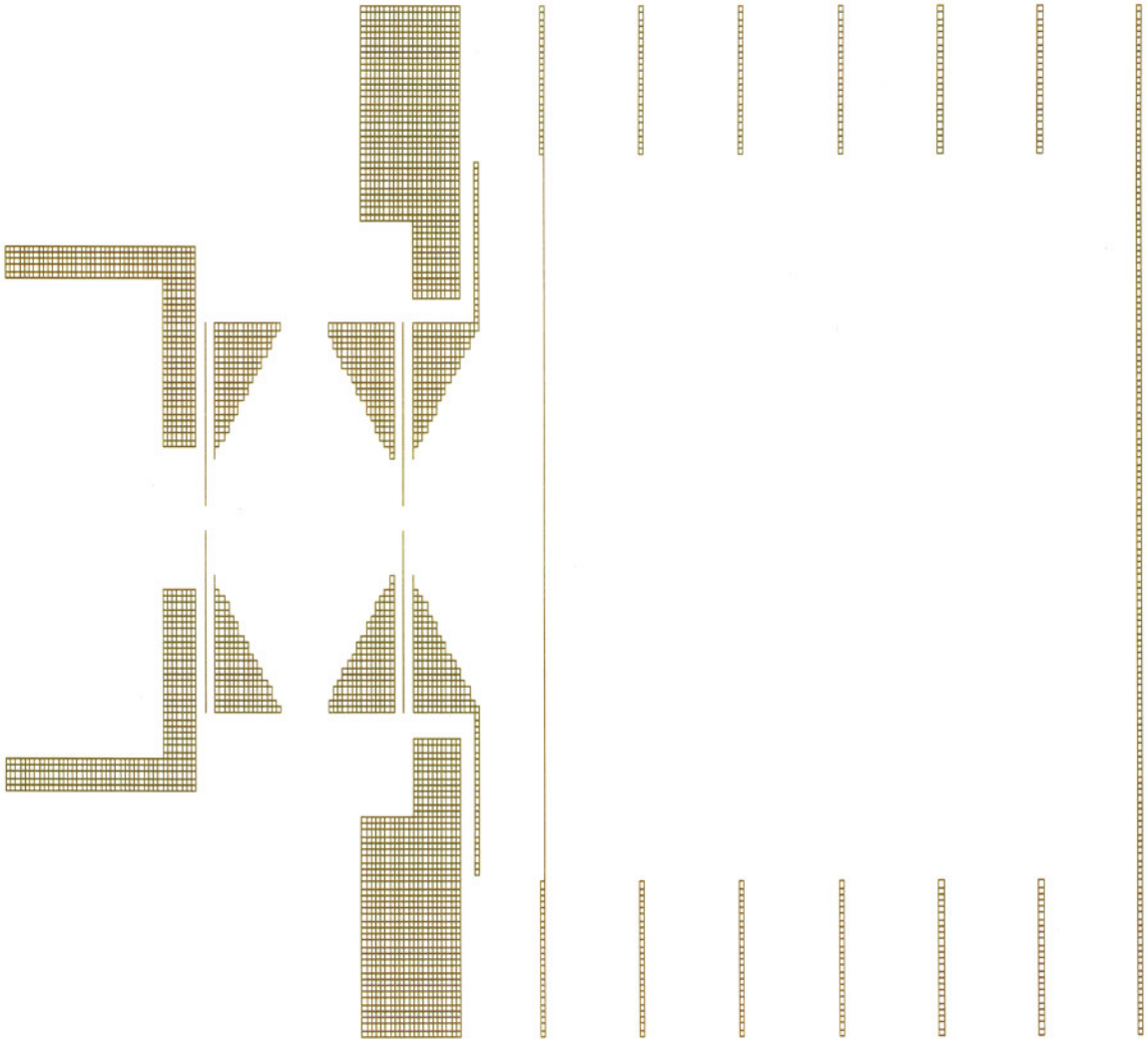

Figure 6: Modified Split field drift tube.

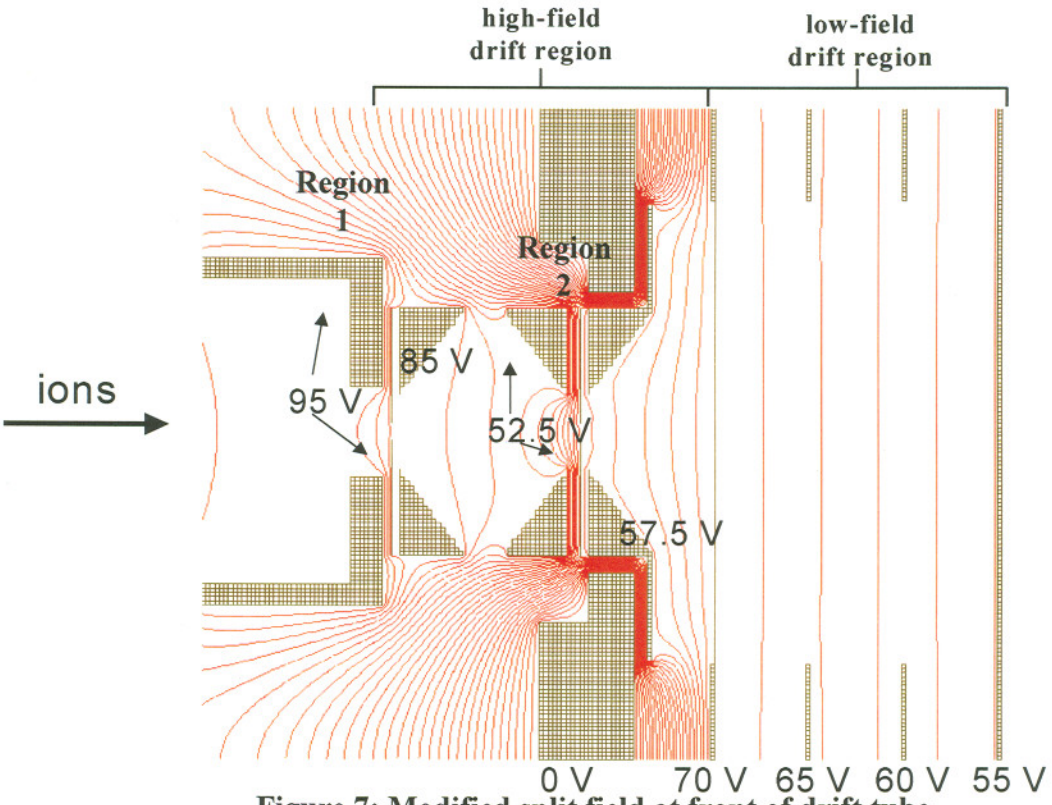

Figure 7: Modified split field at front of drift tube.

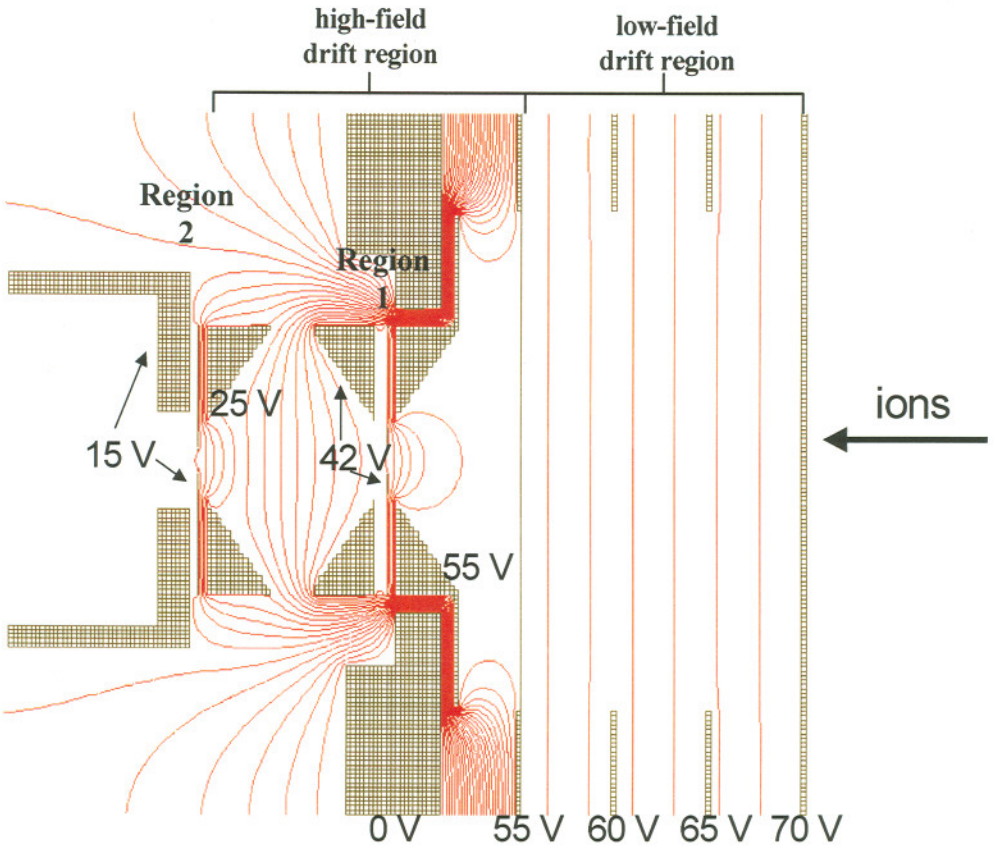

Figure 8: Modified split field at rear of drift tube.

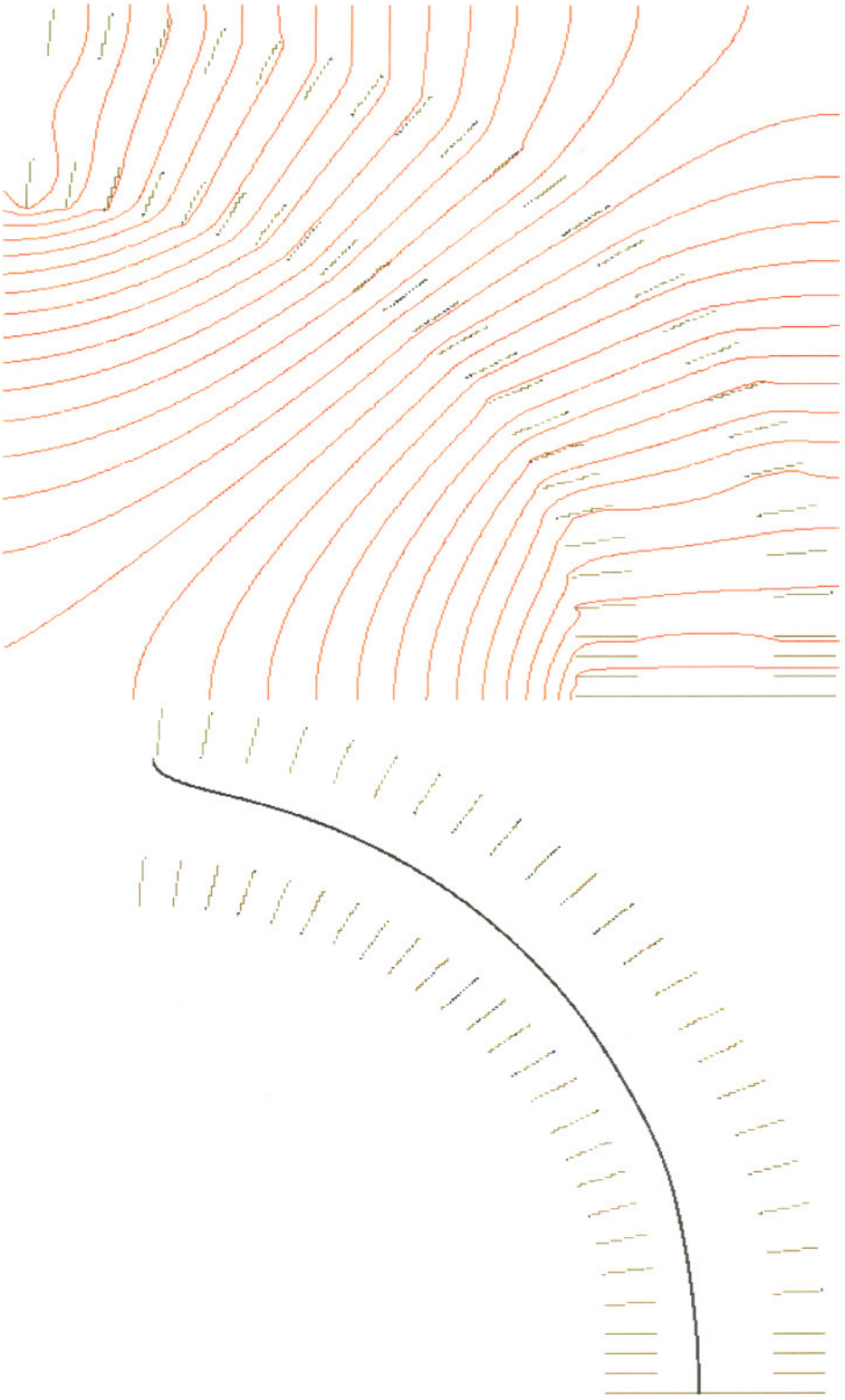

Figure 9: Field lines and ion trajectories for curved drift tube using a four-degree spacer.

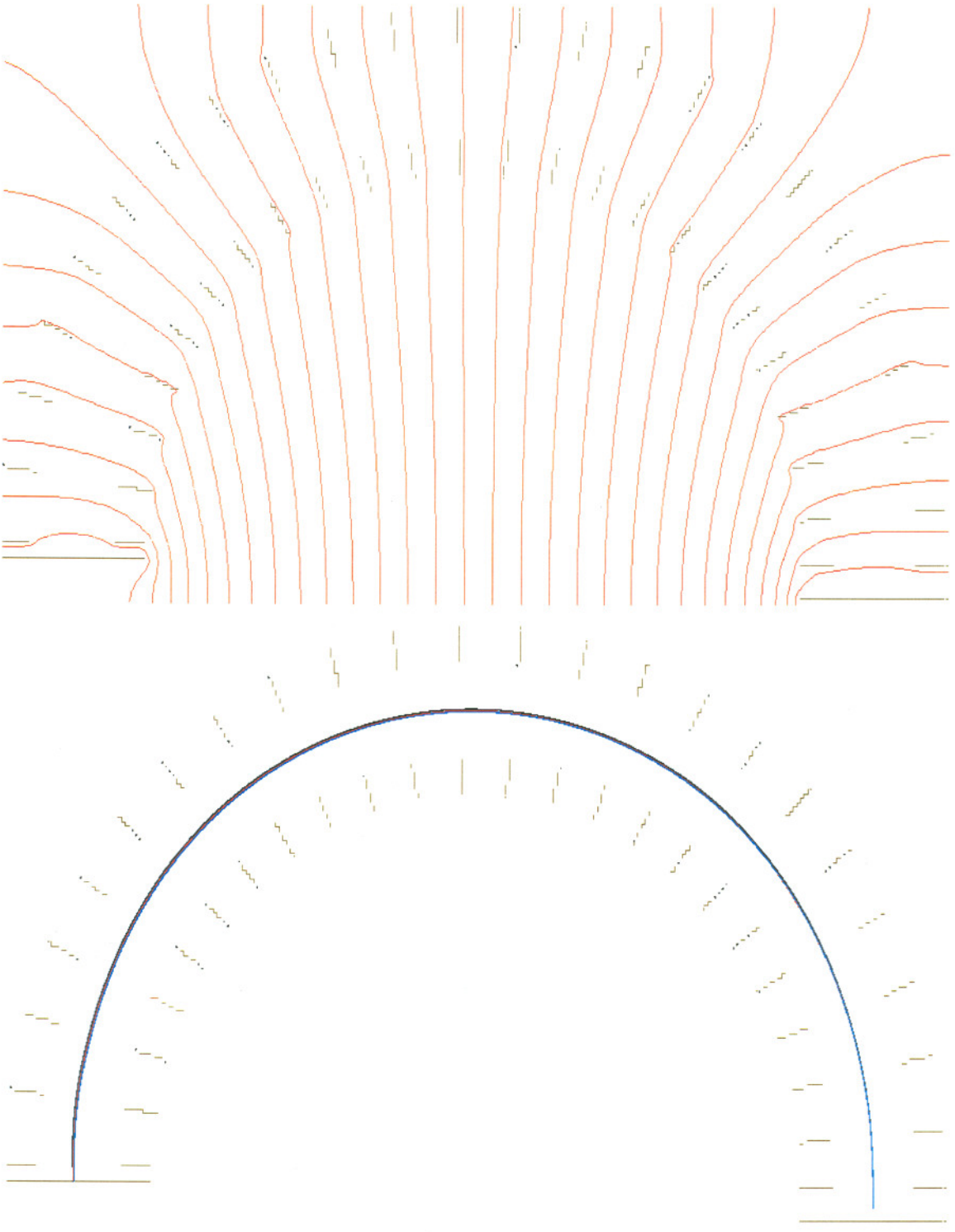

Figure 10: Field lines and ion trajectories for curved drift tube using an eight-degree spacer.

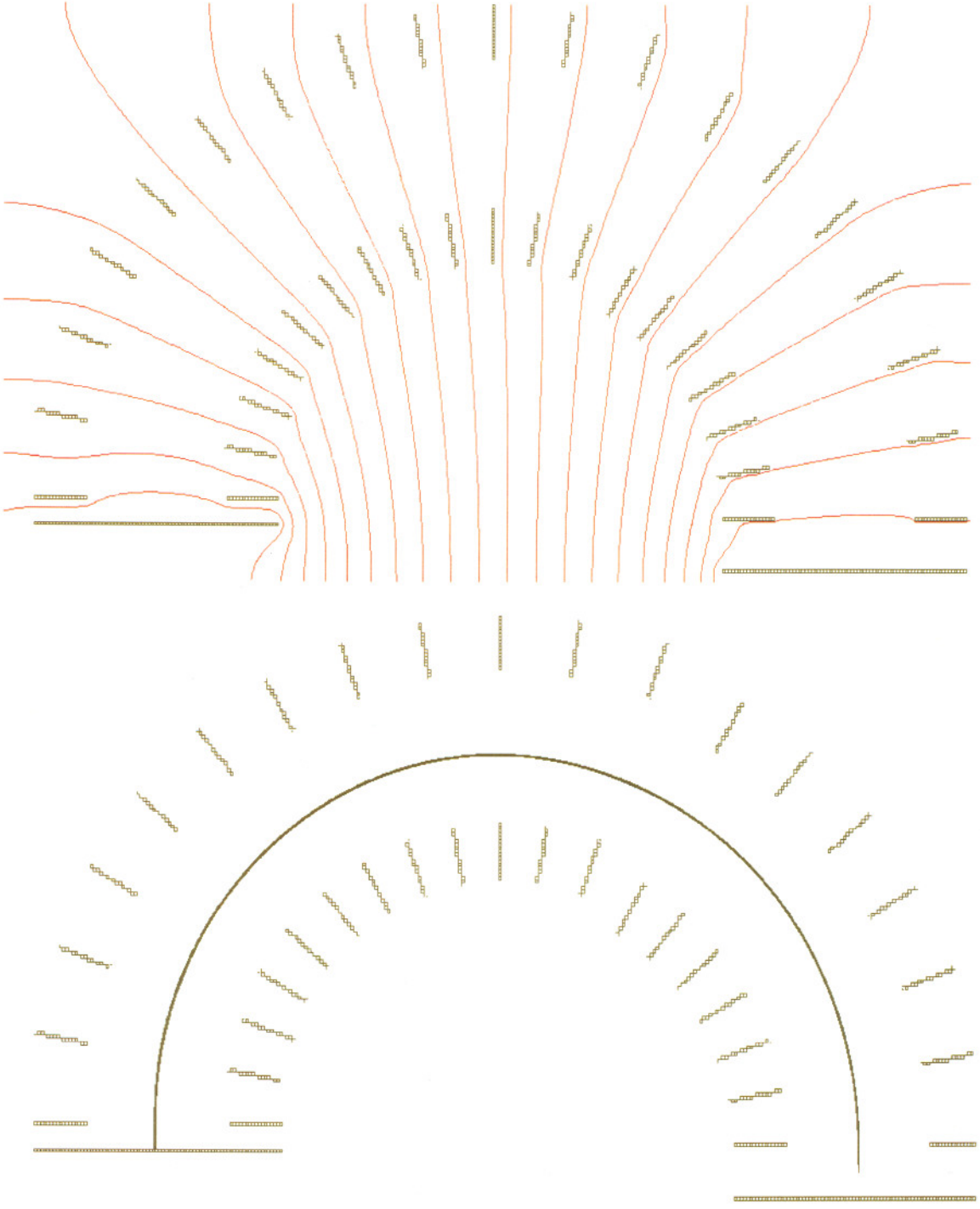

Figure 11: Field lines and ion trajectories for curved drift tube using a ten-degree spacer.

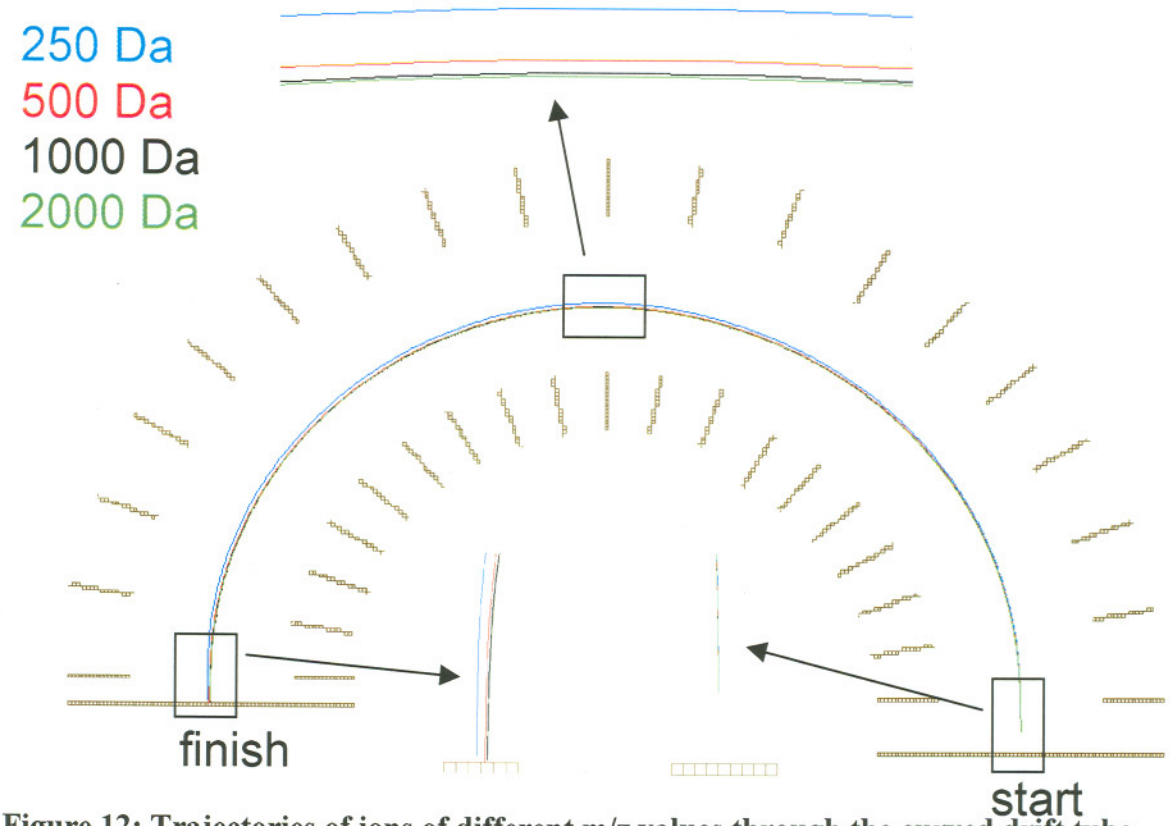

Figure 12: Trajectories of ions of different m/z values through the curved drift tube.

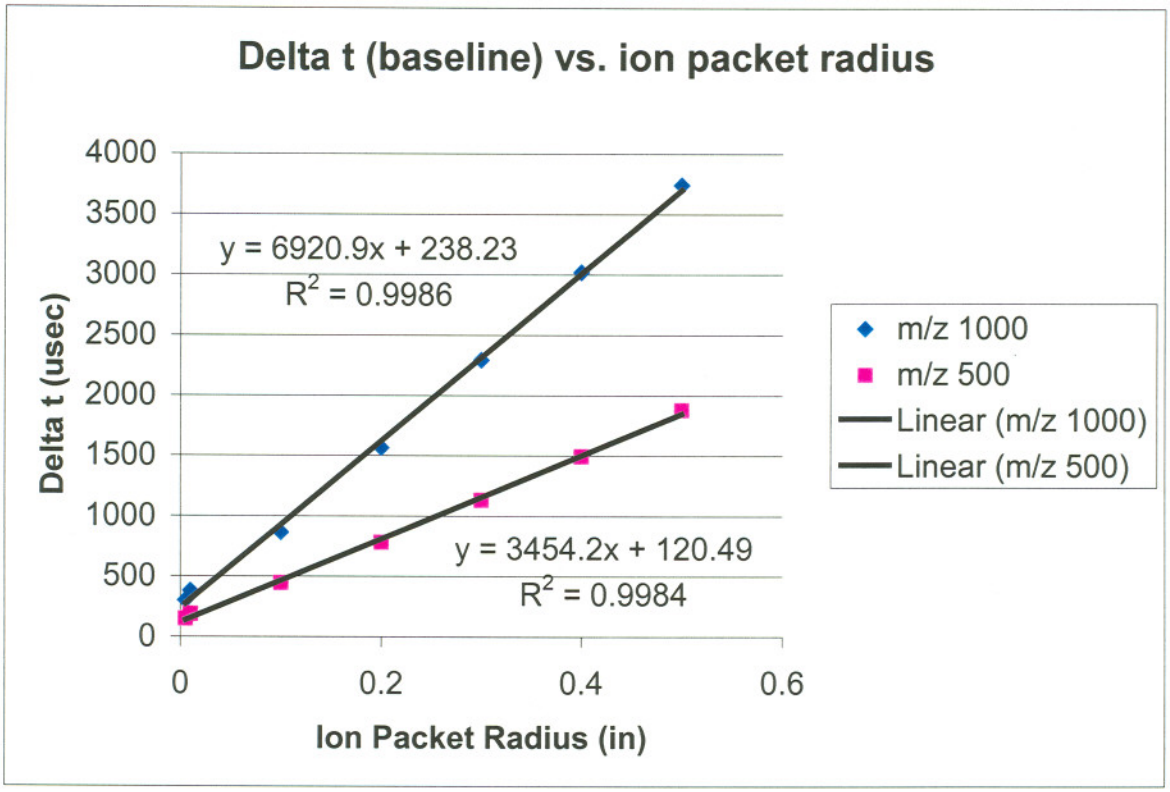

Figure 13: Effect of ion packet width on temporal resolution in curved drift tube.

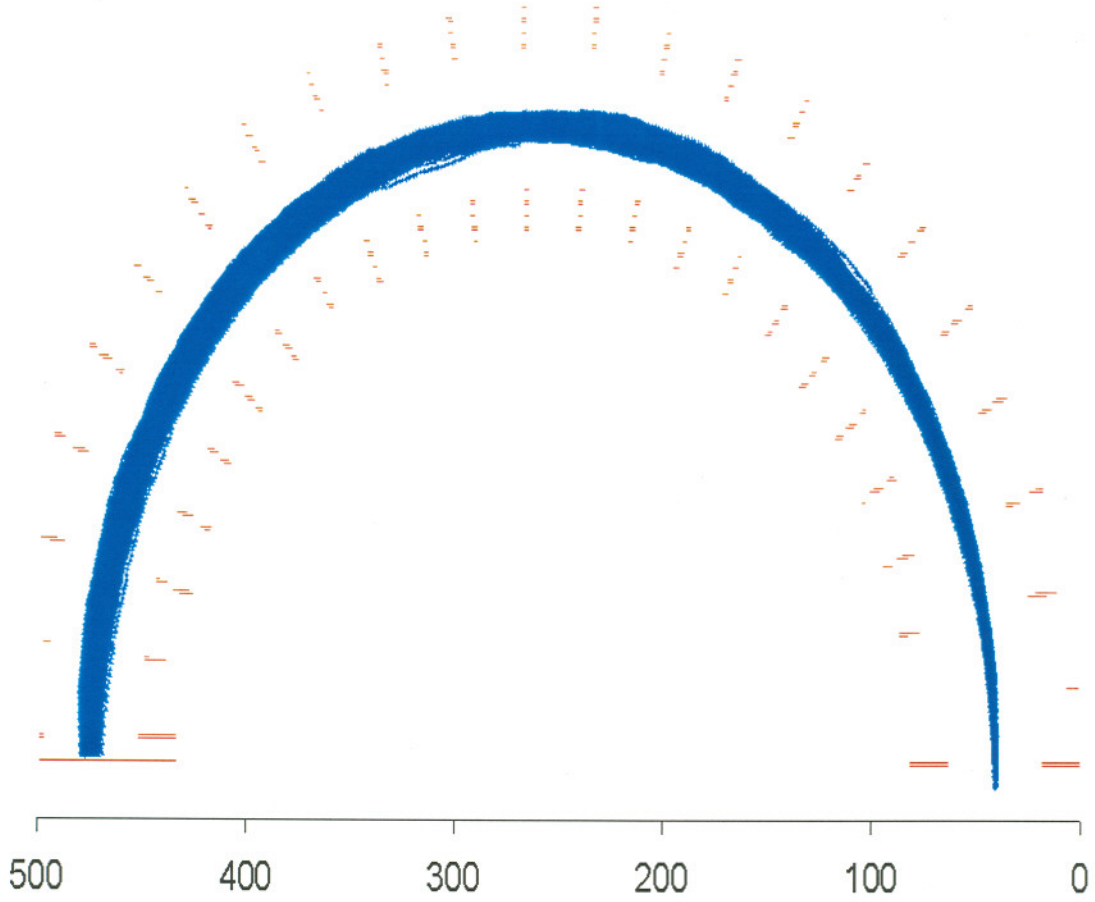

Figure 14: Effect of diffusion on width of ion packet in curved drift tube.

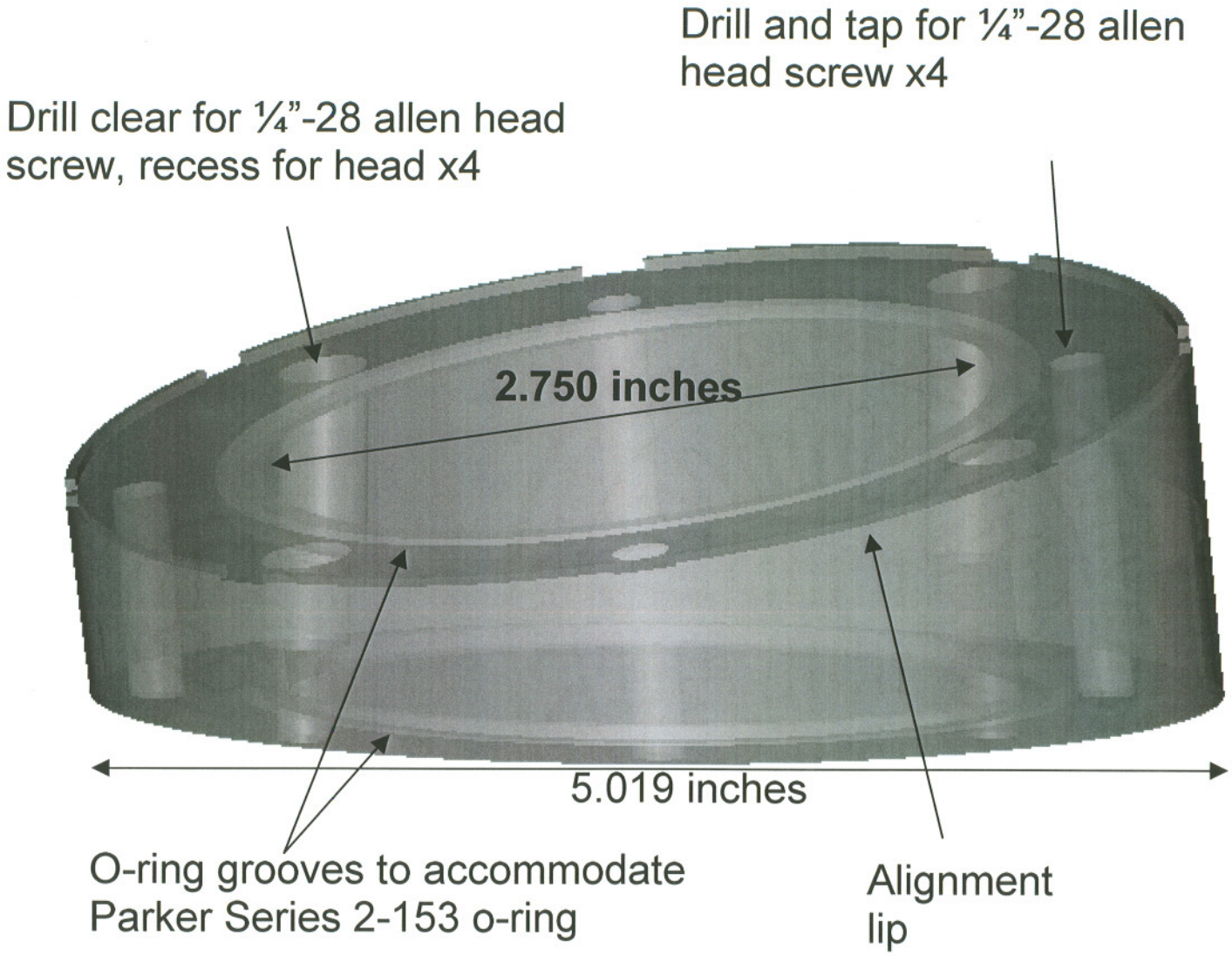

Figure 15: MasterCam design drawing of first curved drift tube spacer.

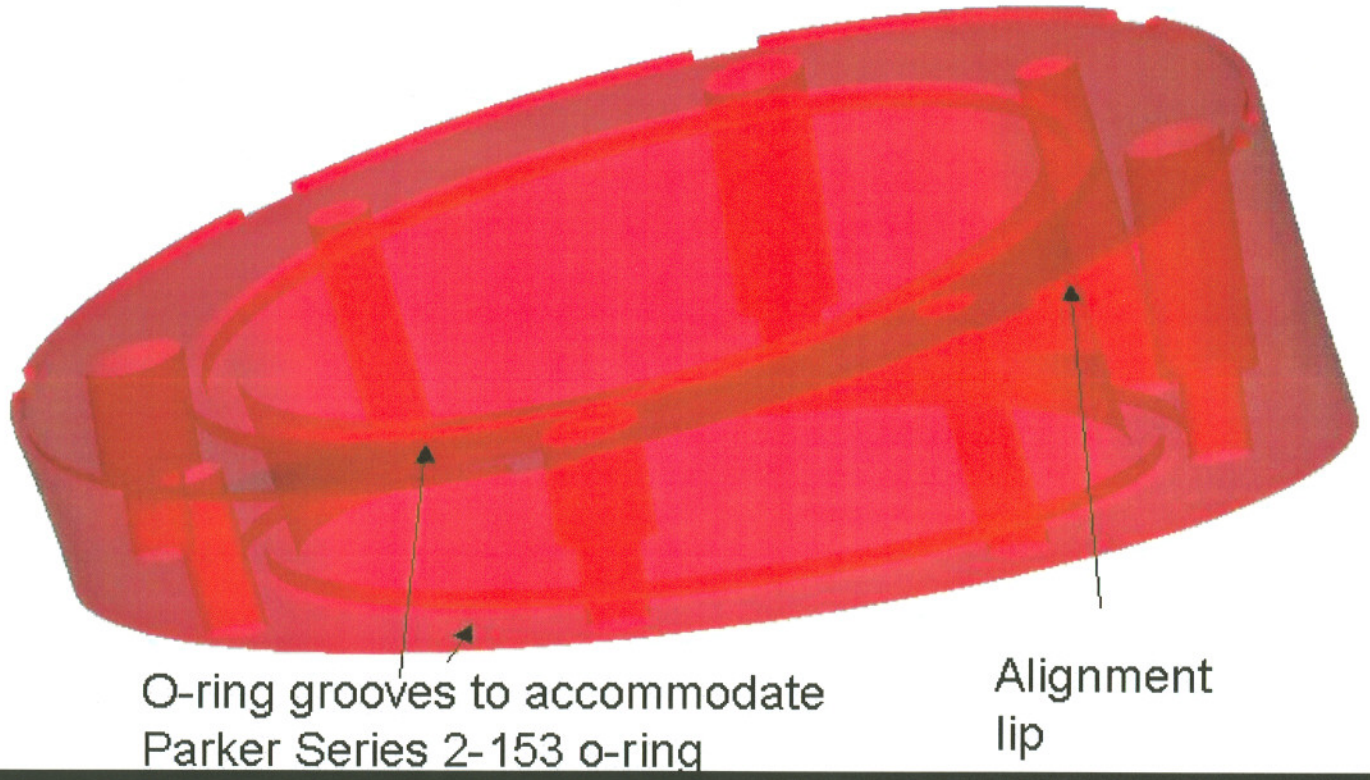

Figure 16: MasterCam design drawing of second curved drift tube spacer. Dimensions same as Figure 18. Notice that the bolt holes are offset by ninety degrees from the first spacer.

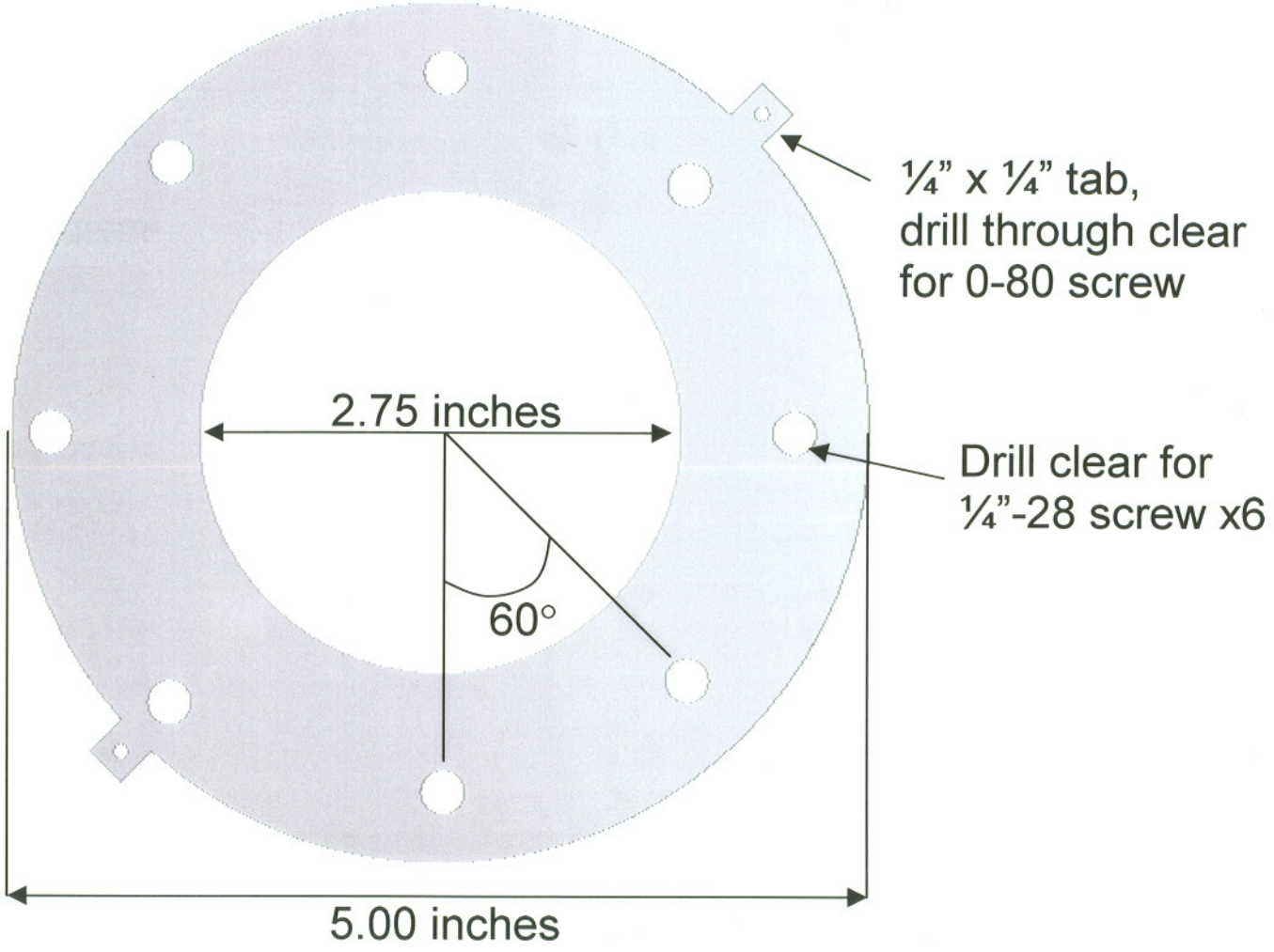

Figure 17: Curved drift tube electrode.

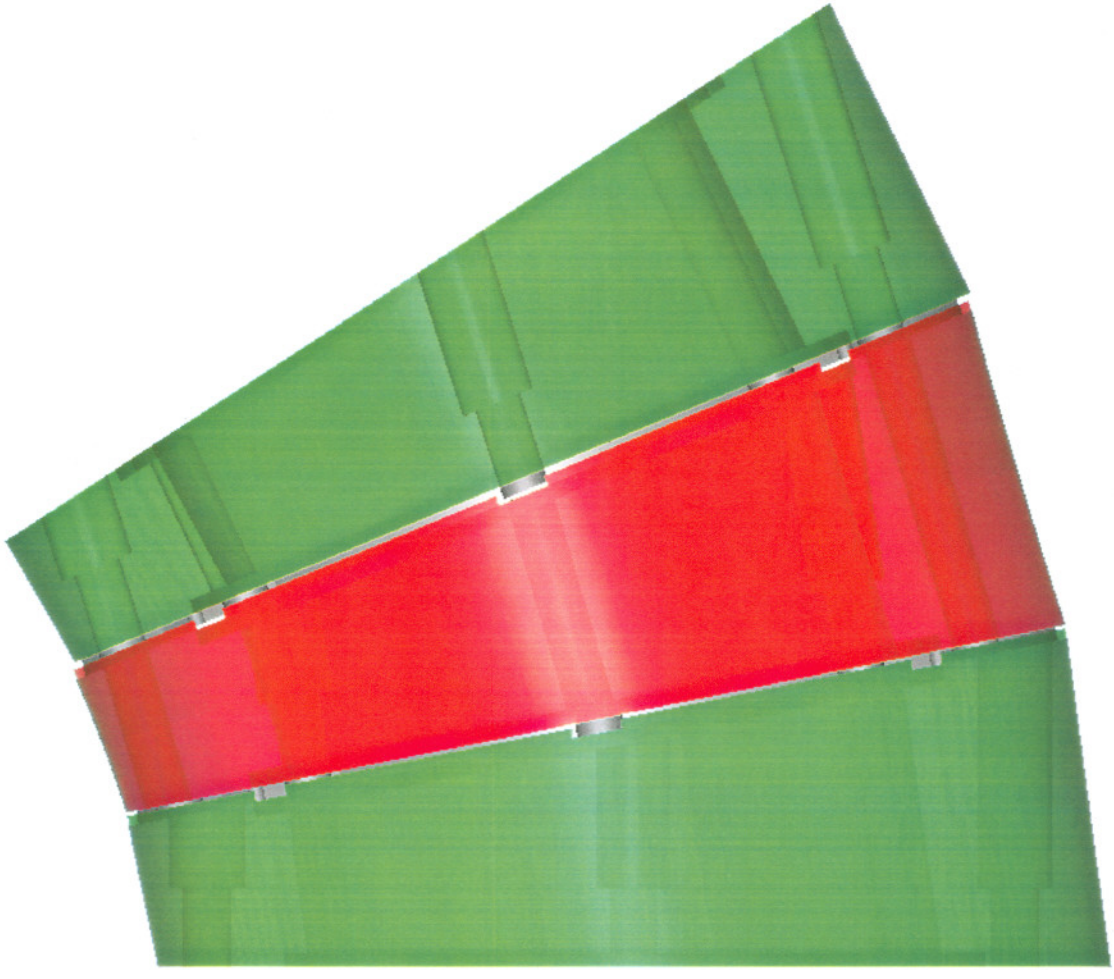

Figure 18: MasterCam draft displaying connectivity of drift tube spacers.

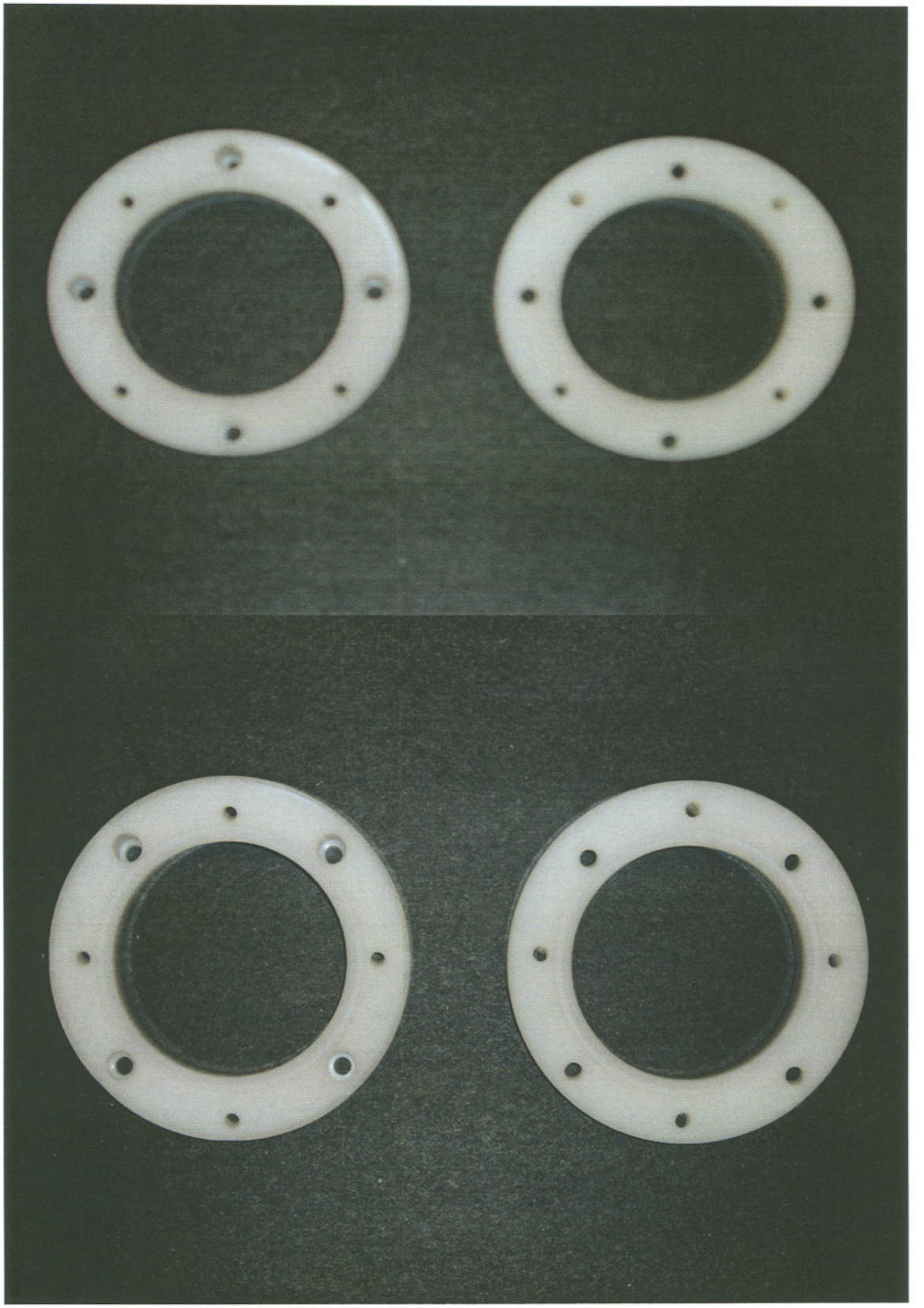

Figure 19: Photographs of curved drift tube spacers.

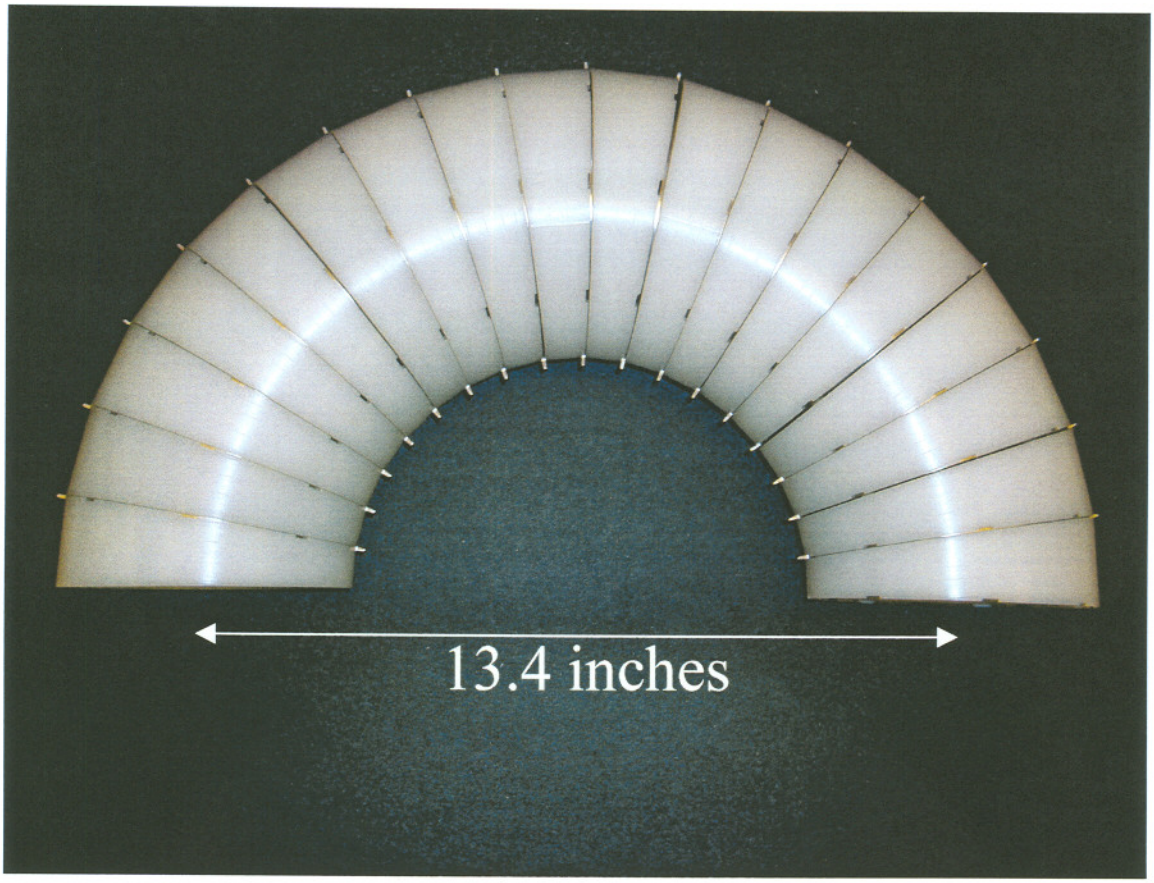

Figure 20: Photograph of assembled curved drift tube.

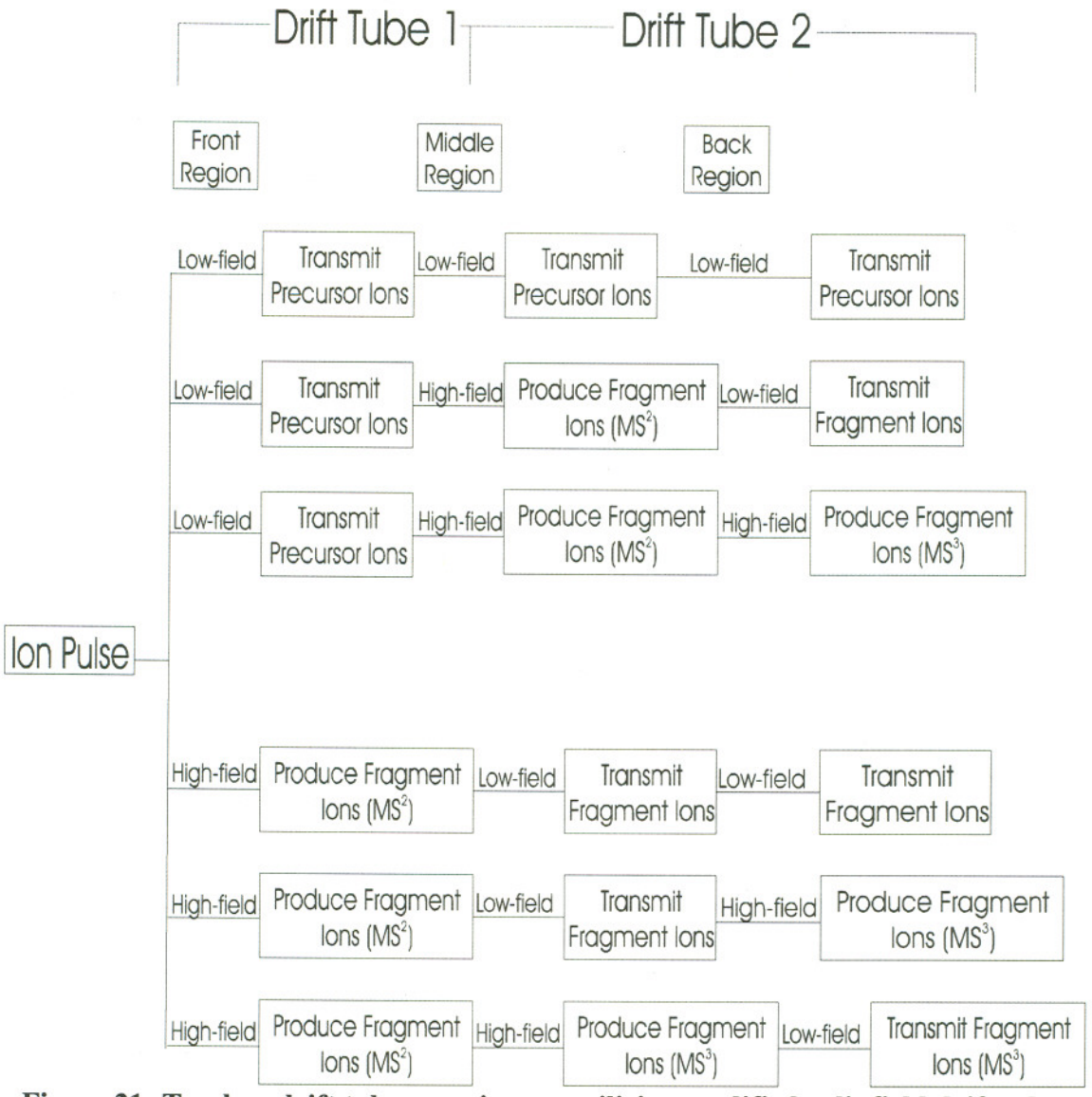

Figure 21: Tandem drift tube experiments utilizing modified split field drift tube.

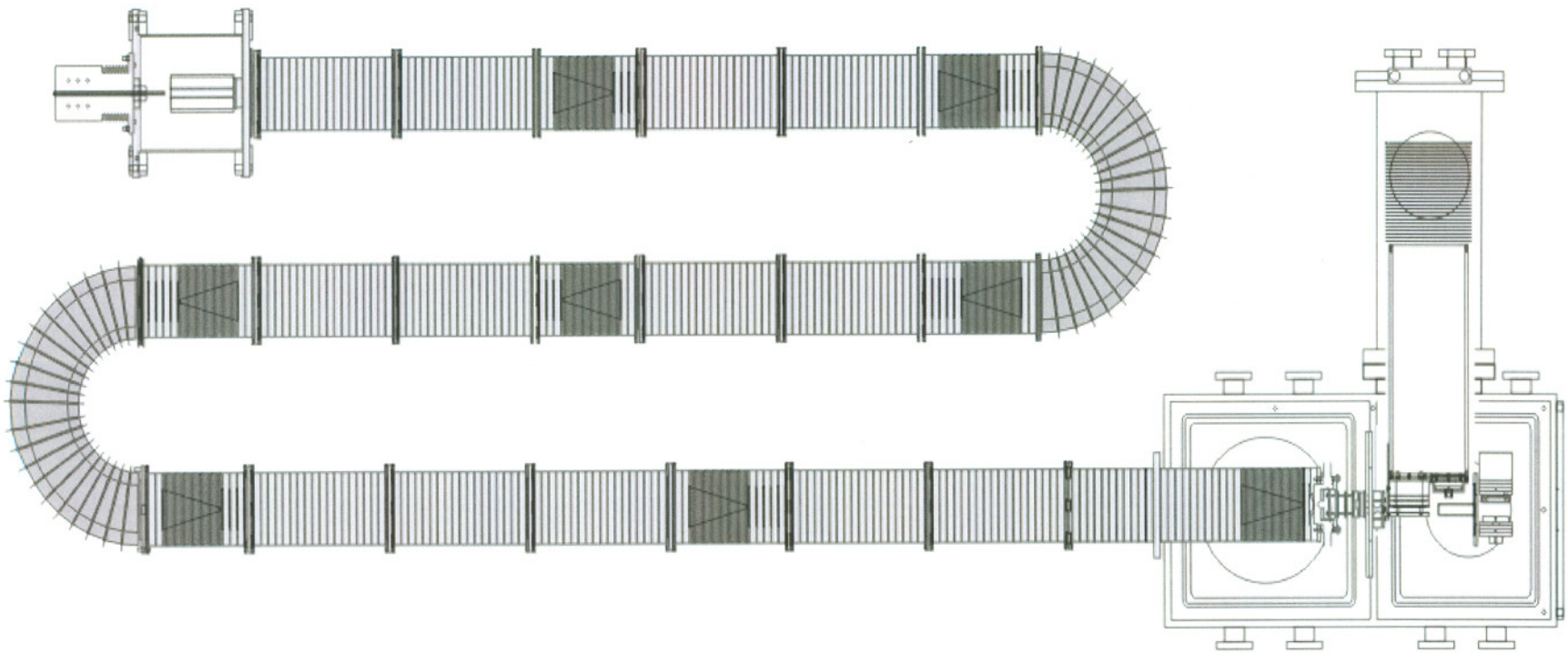

Figure 22: Schematic diagram of high-resolution long length drift tube.

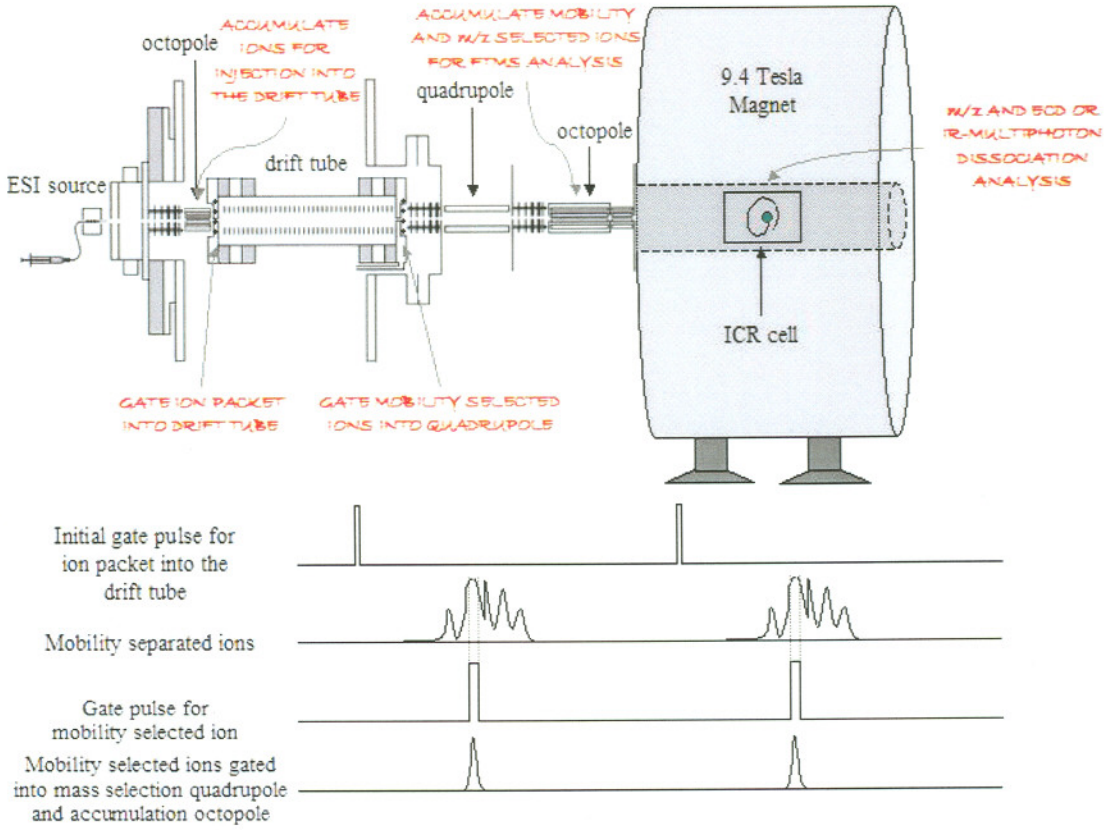

<u>Figure 23:</u> Schematic diagram of drift tube/FT-ICR MS instrument to be built in conjunction with the Marshall lab at Florida State University.